CHAPTER 5

NON-LINEAR FINITE ELEMENT ANALYSIS FOR SFRC BEAM

5.1 Introduction

In this chapter, a brief description for the finite element programme is presented. The σ-ε relationship is determined for SFRC containing 15 kg/m^3 of hook-end steel fibres using the proposed analysis method explained in chapter 4. A non-linear finite element model is proposed to analyse the SFRC beam using the calculated σ-ε relationship. The results from the finite element analysis are tested by comparison to experimental results presented in section 3.4. The aim of this chapter is to determine and test the σ-ε relationship that will later be used to analyse a SFRC ground slab manufactured using the same materials.

5.2 A brief description of the finite element programme

The MSC.Marc is a general-purpose finite element programme. It has the capability to analyse SFRC structures by utilising the cracking model for low-tension materials. This cracking model adopts single fixed crack formulations. Accordingly, a crack develops at an integration point perpendicular to the direction of the maximum principal stress if the maximum principal stress in the material exceeds the specified value. After an initial crack has formed, a second crack can form perpendicular to the first crack. For perfectly smooth crack surfaces this assumption is always correct, but if some residual shear stiffness is introduced, the cracks might occur at other angles. The cracking model implemented in MSC.Marc does not cater for such effect. It is worth noting that the choice of the single-fixed crack approach was made based on the availability of the finite element programme.

The material loses all load-carrying capacity across the crack unless tension softening is included. Stresses are transmitted between the crack faces according to the softening part of the σ-ε response. These stresses diminish until there is no stress across the crack, thus no load carrying capacity exists in tension. After crack formation, the loading can be reversed due to the redistribution of stresses. In this case, the crack can close again, and partial stitching occurs. After load removal all strains return to zero as indicated in Figure 5-1. When stitching occurs, it is assumed that the crack has full compressive stress-carrying capability. In the analysis, provision is made for the compressive strains to increase beyond the yield point. In this case, it is necessary to combine the material model with yielding criteria defining the multi-axial stress state. The programme provides

several mathematical models to describe the yielding surface for concrete that can be incorporated into the analysis. In analysis involving compression-compression and tension-tension, the yield surfaces can be combined with crack detection surfaces to describe both the cracking and yielding behaviour of the material.

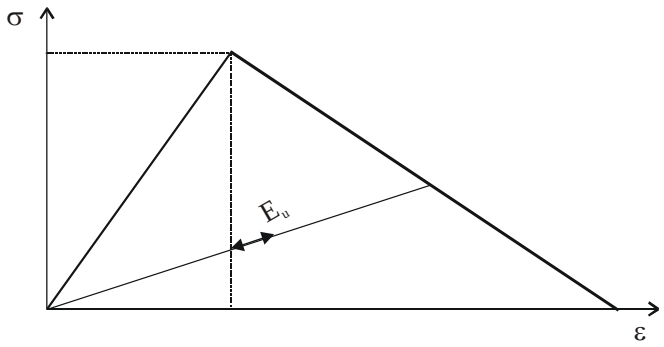

Figure 5-1: Unloading behaviour adopted in MSC.Marc.

The softening behaviour is characterised by a descending branch in the tensile σ-ε response. The cracks at an integration point are uniformly distributed (smeared) over the area representing the integration point. In view of that, the choice for the element size is vital to the results of the analysis as the softening behaviour is dependent upon the fracture energy released after initiation of cracking. In the programme, provision is made for input of a linear softening response. However, the linear softening response is expandable to a bilinear or higher order response by writing special subroutines as permitted in the programme.

The non-linear finite element analysis requires that the tolerance on convergence as well as the maximum and minimum number of recycles needed to obtain convergence should be specified. Two loading schemes are available, the fixed load increment and the automatic load increment scheme (i.e. arc-length method). Different solution algorithms are available and can be employed in the analysis. If the inputs to the programme are correct, convergence can be obtained by changing the convergence tolerance, load increment scheme, iteration limits or the solution algorithm.

In non-linear finite element analysis, it is necessary to apply the load in increments and let each load increment iterate to equilibrium state, within a specified tolerance, using a particular iteration scheme. In MSC.Marc, the loads can be applied through the use of “time” curves. The “time” value represents a variable, which denotes the intensity of the applied loads at a certain step. The choice of “time” step size depends on several factors such as the level of non-linearity of the problems and the solution procedure. The complete load history can be divided into several phases, where each phase is applied at a specific time in the load history. Each phase applied in a specific time period

can be considered as a load case. In this way, the complete loading history can be defined. Note that a load case is not necessarily identical to a load step. A load case may consist of several load steps to reach the total load of the load case.

5.3 Stress-strain relationship

The method proposed in chapter 4 is utilised to calculate the σ-ε response using the measured P-δ response for SFRC beam containing 15 kg/m^3 of hook-end steel fibres. The concrete mix, test setup and testing procedure are presented in chapter 3. A summary of the beam properties utilised in the analysis are indicated in Table 5-1.

Table 5-1: Properties used in the numerical analysis

Property	Value	Remark
Young's modulus	28 GPa	Measured (*)
Cube strength	45 MPa	Measured (*)
Poisson's ratio	0.2	Assumed
Form factor for shear	6/5	Square section

(*) Average value

A first estimate of the tensile σ-ε relationship is shown in Figure 5-2 (a). The first estimation is made based on the recommendations presented in section 4.3.5. The calculation using this response is presented in Appendix C. The P-δ response using the first estimate is presented as dotted curve in Figure 5-2(b).

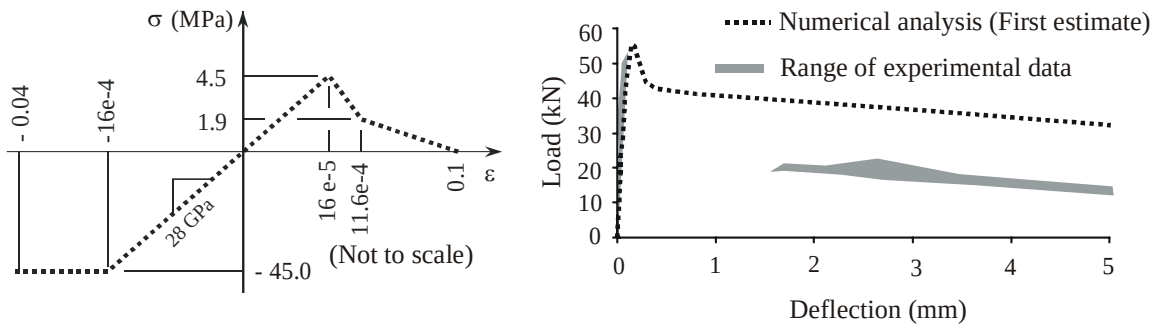

(a) First estimate for the stress-strain response

(b) Comparison between calculated and measured load-deflection responses

Figure 5-2: First estimate for the stress-strain response for SFRC.

Figure 5-2(b) shows that the first estimate for the σ-ε relationship results in a peak load that is slightly high while the elevation of the third segment of the P-δ response is too high. In the light of the parameter study presented in chapter 4, the first adjustment is done to the P-δ response by reducing the value of residual stress (σ_{tu}). A trial-and-error procedure is followed until the correct elevation of the third segment of the curve is maintained. In the second step, the peak load is decreased by reducing the value of the cracking strength (σ_{t0}). Finally, a reasonable match between theoretical and experimental P-δ responses is achieved by minor changes in the values of the residual strain (ε_{t1}) and the ultimate strain (ε_{tu}). The strategy to be followed for the trial-and-error procedure is to apply a coarse reduction or increase step to the specific parameter while using finer steps towards the close matching for the particular part of the adjusted curve. The adopted σ-ε relationship and the calculated P-δ responses are shown in Figures 5-3 and 5-4 respectively. Close agreement is found between the analytical and experimental results. Refer to Appendix C for the calculation of the adopted σ-ε response.

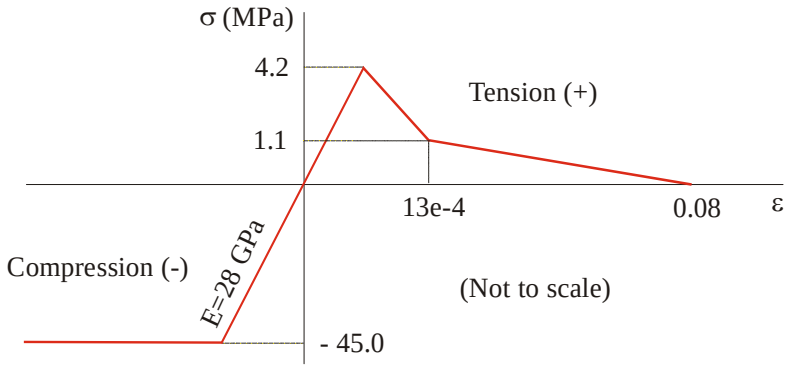

Figure 5-3: Calculated stress-strain response for SFRC (15 kg/m^3 hook-end steel fibres).

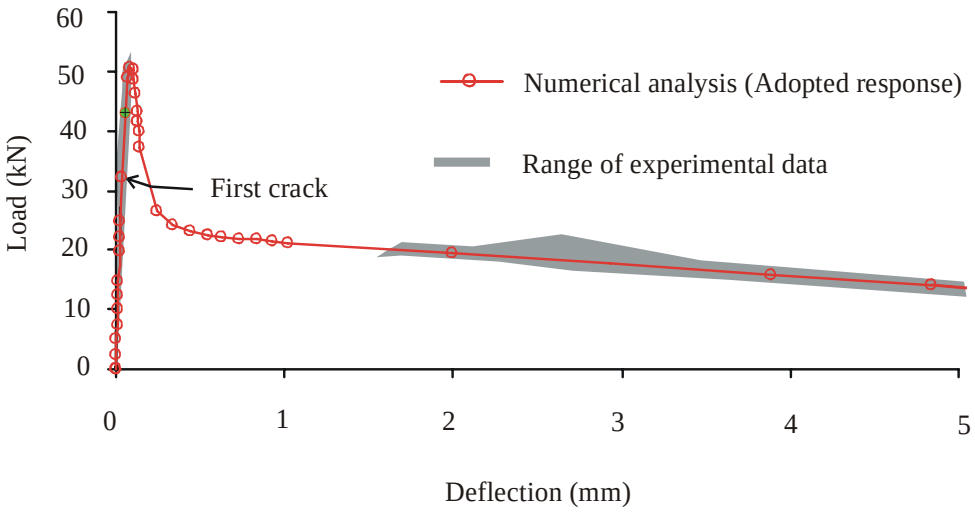

Figure 5-4: Comparison between calculated and measured P-δ responses.

The recommendations presented in section 4.3.5 used to provide the first estimate is found to overestimate the value of σ_{tu} by approximately 70 percent. This can be considered in future analyses when giving initial estimation for the σ-ε response. However, the criterion to estimate the remaining parameters of the σ-ε response is found to be adequate since it provided a close estimation and therefore minor adjustments were required to determine the adopted response.

The analysis has shown that the point where the tensile stress (4.2 MPa) in the material is first reached occurs in the pre-peak regions of the P-δ responses (see arrow in Figure 5-4). This emphasises the fact that elasticity theory under-estimates the load carrying capacity for particular structures. For example, for the analysis conducted here the peak load (52 kN) is higher by approximately 63 percent compared to the load at the first crack (32 kN). Full tensile capacity of the SFRC is only utilised when the analysis proceeds beyond the σ_{t0} point. It is worth mentioning that the peak load on the P-δ response corresponds to a tensile stress located in the part of the σ-ε relationship between ε_{t0} and ε_{t1} (the first branch of the softening curve). These findings correlate well with the analysis presented in section 4.2.4.

Figure 5-5 shows the comparison between the proposed and the output compressive σ-ε responses. The compressive strain exceeds the value for ε_{c0} (= 1.6×10^{-3}) only at the last two points. In the calculated P-δ responses, these two points correspond to deflections that are greater than a deflection limit of 3 mm. The value of 3 mm represents the serviceability limit for deflection for this beam (span/150) as prescribed by the procedure of the Japanese Institute of Concrete (JCI-SF4, 1983). This means that within the desired practical part of the P-δ response, the behaviour is dominated by cracking while the compression side of the beam remains elastic.

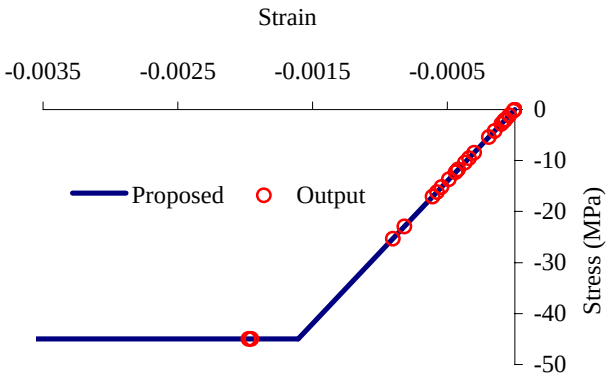

Figure 5-5: Proposed and output compressive stress-strain relationship.

5.4 Finite element analysis of a single element

A special cracking subroutine is developed to enable the input of a bilinear curve for the softening part of the tensile σ-ε response of SFRC (refer to Appendix C). A single element subject to direct tension is analysed to verify the developed subroutine. The direct tension is necessary to avoid possible crack rotation in the analysed boundary problem. Hence, the numerical simulation of the single-fixed crack approach implemented in the MSC.Marc fits the direction of the physical crack that is expected to occur. If the input and the output σ-ε responses thoroughly match then the developed subroutine is deemed to be correct.

Figure 5-6: shows the single finite element and the boundary conditions. Element type 3 of MSC.Marc is used. It's a four-node quadrilateral element developed for plane stress applications. The displacements of the nodes of one side of the element are fixed in the X and Y-directions while a displacement is applied to the nodes in the opposite side to create the direct tension in the element.

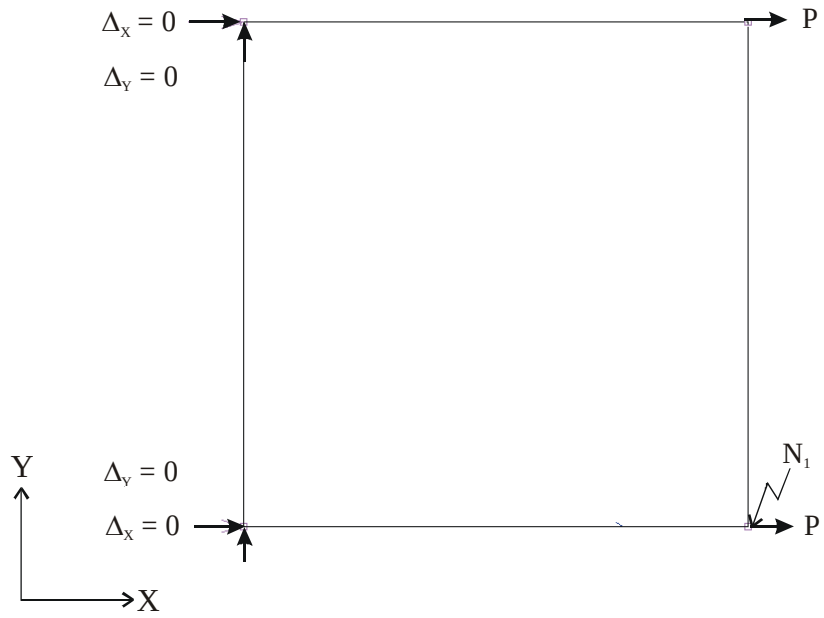

Figure 5-6: The finite element mesh and boundary conditions for the single element.

Figure 5-7 shows the comparison between the input and the output σ-ε responses. The output response is extracted at the integration point corresponding to the node designated (N_1) (refer to Figure 5-7). The input and the output σ-ε responses fits perfectly. The subroutine is shown to be satisfactory and will be used in further analyses involving bilinear softening behaviour.

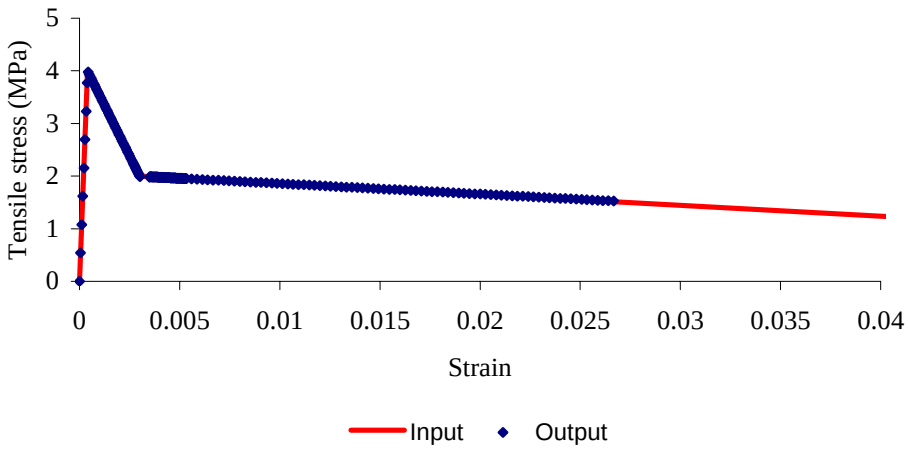

Figure 5-7: Comparison between the input and the output tensile stress-strain responses for the single finite element.

5.5 Finite element analysis of SFRC beam

This section includes the finite element simulation for the SFRC beam discussed in section 5.3. The adequacy of the developed finite element model is tested by comparing the measured and computed P-δ responses. The input and the output tensile σ-ε responses are compared to verify the appropriateness of the single fixed crack approach used in MSC.Marc computer programme.

5.5.1 Geometry and boundary conditions

Because of symmetry, only a half of the beam is analysed. Element type 75 of MSC.Marc is used. It is a four-node thick shell element with six degrees of freedom per node, which are three displacements (Δ_X, Δ_Y and Δ_Z) and three rotations (θ_X, θ_Y and θ_Z). The stiffness of this element is formed using four-point Gaussian integration. The thickness is divided into layers and the stress and stiffness states are calculated at representative points through the thickness. The layer number convention is such that layer one lies on the side of the positive normal to the shell, and the last layer is on the side of the negative normal. The programme requires that the number of layers to be odd and the minimum number of layers is three.

The geometry of the beam is generated using an element size of 150 x 150 mm for the elements to the left of the applied load while an element size of 150 x 75 mm is used for the element to the right of the applied loads (refer to Figure 5-8). The displacements of the nodes representing the left support are fixed in the Y and Z-direction permitting unconstrained expansion of the beam in the

X-directions. The displacement in the X-direction and the rotations about the Y-axis are constrained along the symmetry line of the beam. The displacement in the X-direction of the left support and the rotation about the Z-axis of the nodes along the symmetry line are constrained to prevent rigid body movement (see Figure 5-8).

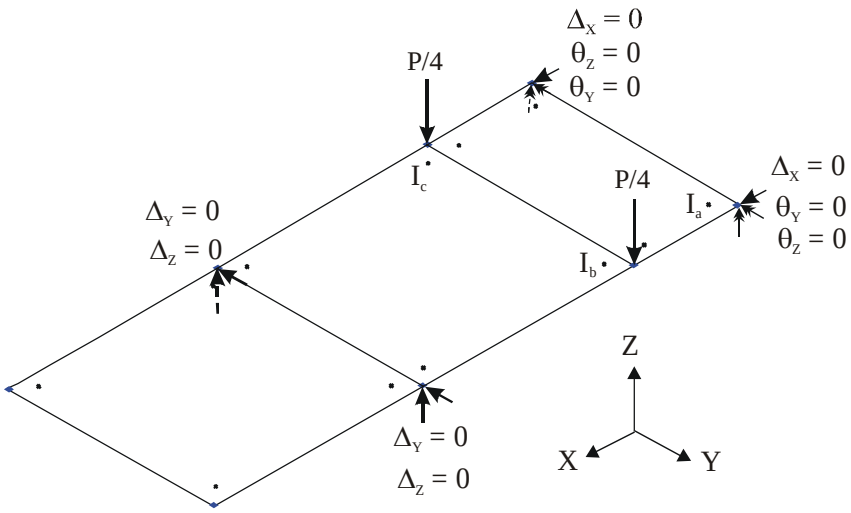

Figure 5-8: The mesh and boundary conditions for the beam.

The displacement controlled loading is simulated by increasing the displacement from zero to -5 mm using the time curve concept. The time is divided into ten-load cases applied consecutively. Each load case is subdivided into a number of load steps, which determine the applied displacement increment. The magnitude of the load steps is varied throughout the loading process to ensure that the resulting P-δ response in the post-cracking region is captured sufficiently. The loading sequence is based upon results of preliminary runs of the model. In the beginning, a single load step is assumed which is further refined based on the coarseness of data points, the calculated P-δ response, the output tensile σ-ε response and the convergence of the solution. This is necessary as the material model includes sharp kinks at which slope change occurs.

5.5.2 Material model for finite element analysis of SFRC beam

The average (or smeared) σ-ε response for SFRC in Figure 5-3 is used. In tension, the maximum principal tensile stress will be limited to the values of this tensile σ-ε response. Once the crack is initiated, the orientation of the crack is fixed throughout the analysis. The tensile strength in a particular direction reduces based on the softening part of the tensile σ-ε response. The crack initiation is governed by the maximum tensile stress criterion, i.e., when the maximum principal

tensile stress exceeds the tensile strength, a crack is formed. Figure 5-5 indicates that the compressive strain falls within the linear elastic region of the compression side of the beam for the desired practical part of the P-δ response. However, for beams or slabs with different dimensions and load setup, the strain magnitude could fall in the non-linear region. To account for all possibilities, the uniaxial nonlinear compressive σ-ε response is adopted for all the finite element analyses conducted in this research. When the principal stress components of SFRC are primarily compressive, the response of the SFRC is modelled by the elastic-plastic theory. The Drucker-Prager compression failure surface, together with a crack detection surface, was used to model the failure surface of the SFRC.

The tensile σ-ε response in Figure 5-3 is determined from the analysis by smearing the crack over the width of the constant moment span (150 mm) of the beam while assuming an infinity number of layers through the depth of the beam. It should be born in mind that objective mesh can only be achieved if the relationship between the element size and the fracture energy is considered. Accordingly the finite element width is chosen as 150 mm while the depth of the beam is arbitrarily divided into eleven layers. Additional analyses are conducted to study the effect of the number of layers in the computed P-δ response.

The fracture energy for the elements having a width of 150 mm is the product of the area under the softening part of the tensile σ-ε curve in Figure 5-3 and the crack smearing width (150 mm). If a smaller or larger finite element size is to be used, the softening part of the σ-ε response will require some adjustment, as the fracture energy should remain unchanged. For example, for a smaller element size the area under the softening part of the σ-ε response needs to be increased until the product of the element width and the calculated area equals the fracture energy for element size of 150 x 150 mm. The use of larger element sizes will require a reduction in the area below the softening part of the σ-ε response.

For the same material, the fracture energy for an element having a width of 75 mm is double to that of an element having a width of 150 mm. In this analysis the tensile σ-ε response in Figure 5-3 is also applied to the element having a width of 75 mm. This is because only half of the beam is modelled and therefore half of the fracture energy will be dissipated while cracking occurs in the half of the constant moment zone of the beam. This would result in the same amount of fracture energy if the full beam is modelled and an element having a width of 150 mm is used in the constant moment zone.

In this analysis, the cracks are expected to only occur in the constant moment zone in which the shear force is zero. Accordingly, a zero shear retention factor should be appropriate, as no shear stresses are transmitted across these cracks. An arbitrary shear retention factor of 0.5 is chosen for this analysis to avoid numerical instability that may arise when using a zero shear retention factor.

5.5.3 Results of the finite element analysis of the SFRC beam

Figure 5-9 shows the deformed shape of the beam. The finite element to the right of the load has displaced in the negative Z-direction and rotated about the Y-axis. The maximum displacement occurs in the nodes positioned at the symmetry line. On the other hand, the finite elements to the left of the load have rotated about the node representing the support resulting in the inner element displacing in the negative Z-direction while the outer element displacing in the positive Z-direction.

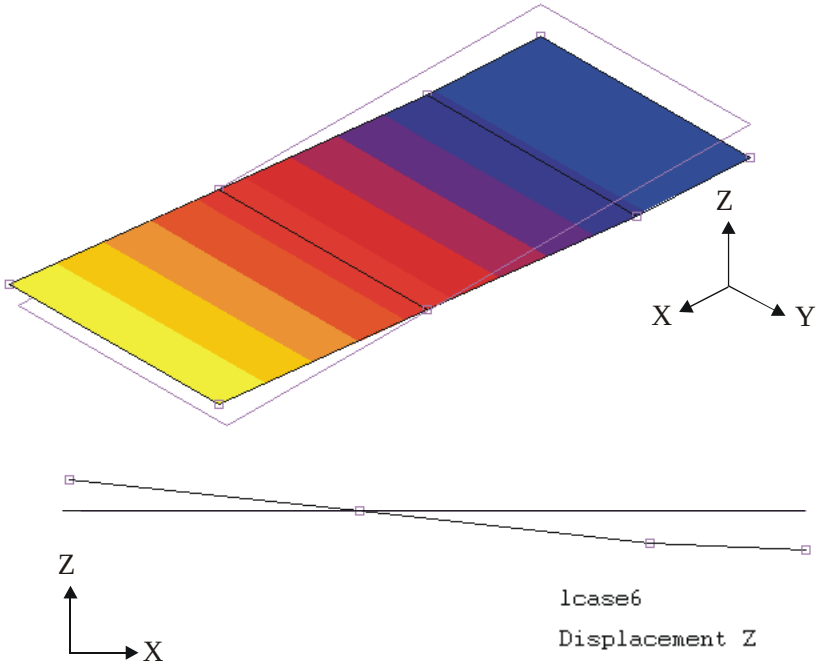

Figure 5-9: The deformed shape of the beam.

Figure 5-10 shows the comparison between the computed P-δ response, obtained using the developed finite element model, and the experimental results. The computed P-δ response is generated by plotting double the sum of the reactions at loading points versus the vertical (Z-direction) deflection at the nodes of the symmetry line for the consecutive increments. The computed and the measured P-δ responses show a reasonable correlation.

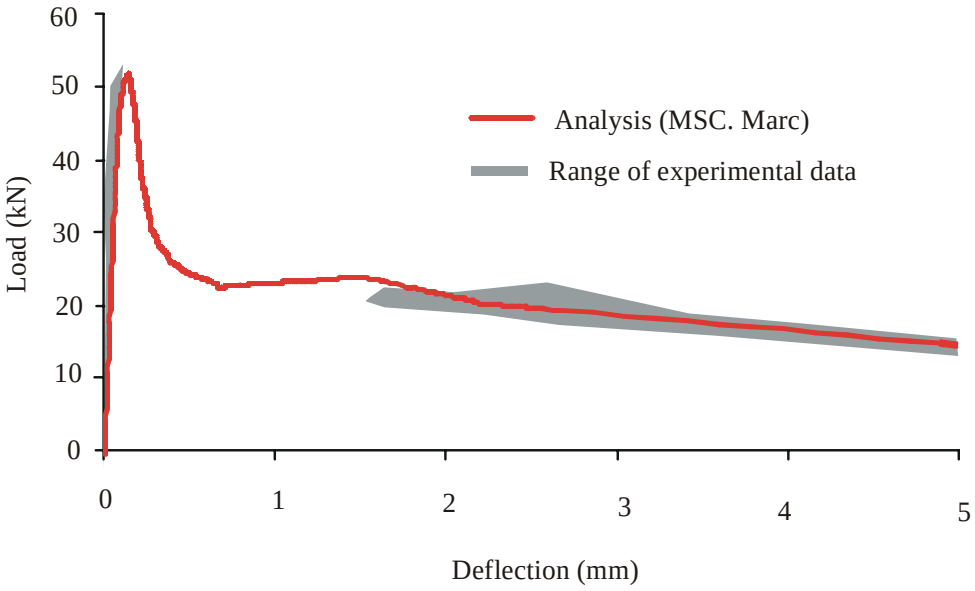

Figure 5-10: Comparison of calculated and measured load-deflection responses - finite element analysis.

Figure 5-11 shows the effect of the number of the layers through the depth of the beam. The use of eleven layers seems to be appropriate for the analysed SFRC beam as the use of 21 layers does not result in a significant change in the *P*-δ response. On the other hand, the use of five layers is found to provide a reasonable match to the *P*-δ response determined using eleven layers except that a second hump is present when using five layers. However, experimental data were not available at the region where the hump occurs and therefore it is not possible to verify if a second hump actually exists. It should be born in mind that the use of more layers allows better representation of the constitutive through the depth of the beam but the economy of the analysis needs to be considered.

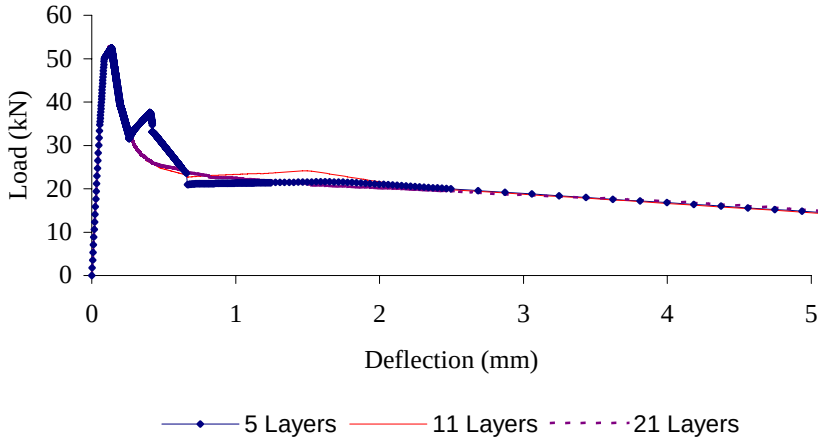

Figure 5-11: Effect of the number of layers on the load-deflection responses.

Figure 5-12 and Figure 5-13 show the distribution of the strains and stresses through the thickness of the analysed SFRC beam. The linear strain distribution correlates well to the assumption made for the numerical method used to determine the tensile σ-ε relationship. The stress distribution shows that the σ-ε relationship is reasonably represented through the depth of the beam. The analysis also shows that no plastic deformation has taken place in the compression side of the beam as the compressive strain and stress are below the value of 1.6 x 10^{-4} and 45 MPa respectively. This correlates well with the results in Figure 5-5 and to the findings of the studies conducted by Hannant (1978), Kooiman et al. (2000) and Robins et al. (2001).

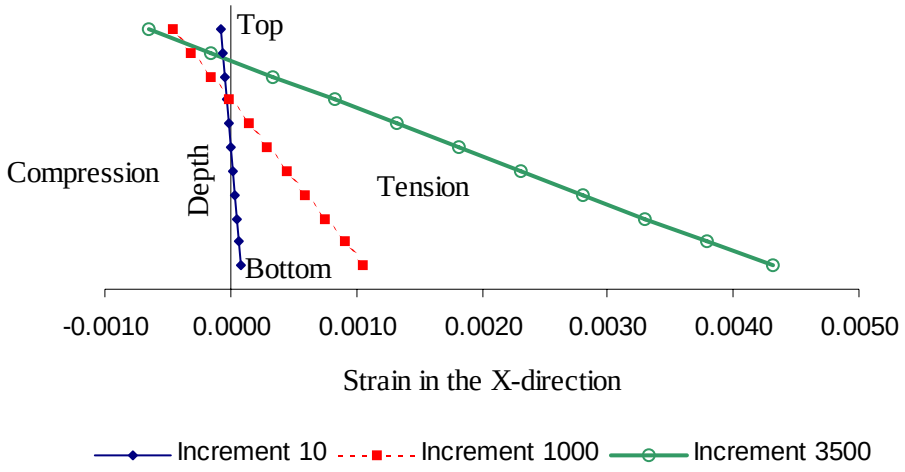

Figure 5-12: Distribution of the strains through the depth of the beam.

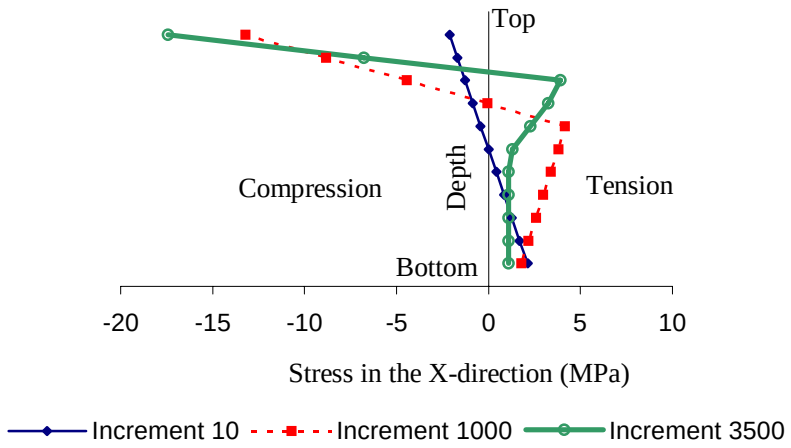

Figure 5-13: Distribution of the stresses through the depth of the beam.

Figure 5-14 shows the comparison between the input and the output σ-ε responses extracted at the integration point (I_a) with respect to the layers 11, 10 and 9 through the depth of the beam. At the integration point, the output and the input responses are found to correlate well. Except for the layer 11 in the part of the curve beyond tensile strains of 0.004 where the input and output tensile σ-ε response diverges. This seems to be caused by the numerical simulation used in which the direction of the crack is fixed once the crack initiates (single-fixed crack approach). The rotating crack approach is not implemented in the MSC.Marc (2003) and therefore it is not possible to fully verify the cause of this difference.

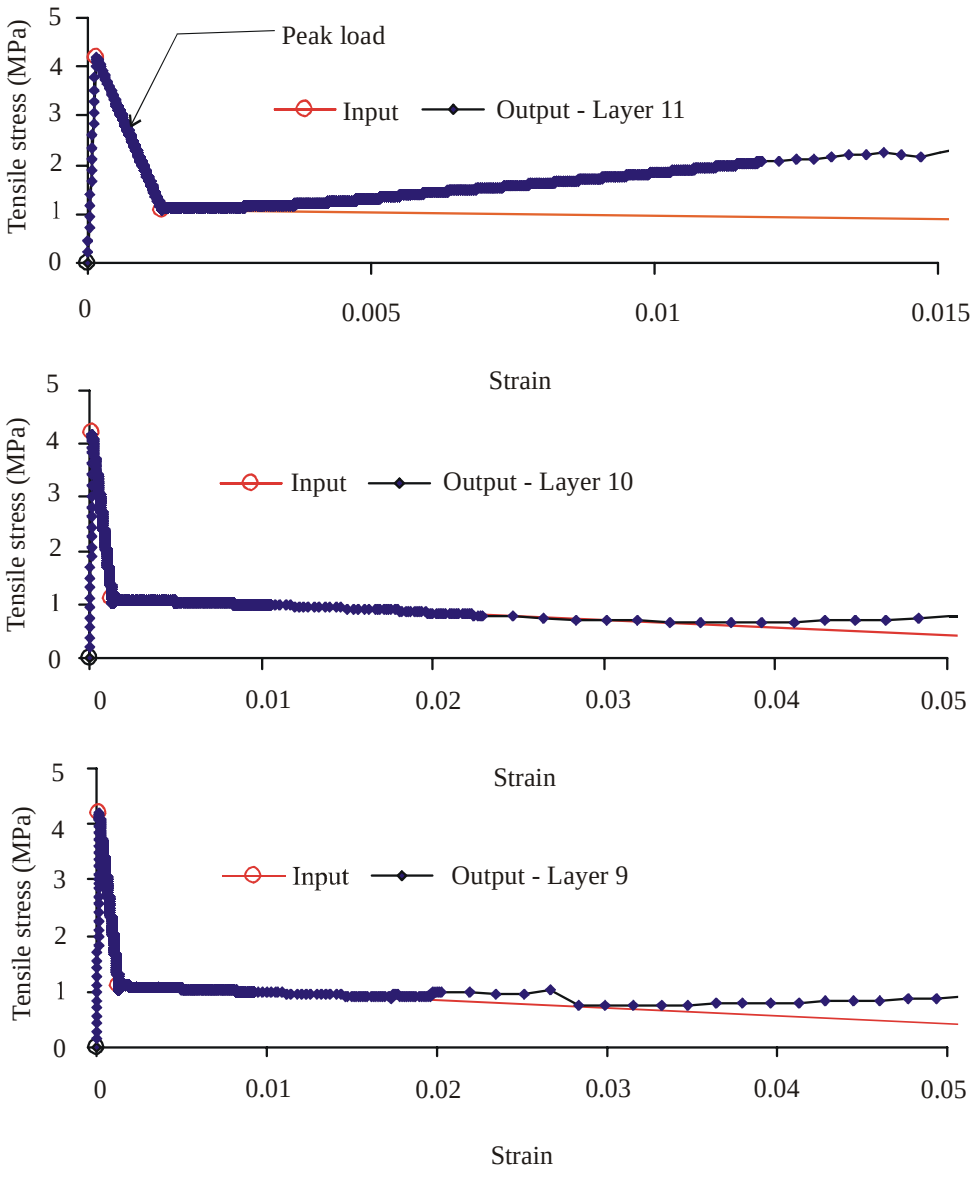

Figure 5-14: Comparison between the input and the output tensile stress-strain responses.

The finite element analysis has shown that the point where the cracking stress in the material is reached occurs in the pre-peak regions of the P-δ response and thus the peak load occurs in the post-cracking region of the σ-ε response (see arrow in Figure 5-14). This result confirms the findings of the numerical analysis presented in section 5.3 and shows the value of incorporating non-linear finite elements in the analysis of SFRC.

Figure 5-15 shows the status of tensile stress in the elements to the left of the loading point. The tensile stresses were found to be less than the cracking stress at integration points named as (I_b) and (I_c) (see Figure 5-8). This indicates that the boundary value problem has enforced localisation of the crack in a single column of elements and therefore the prescribed fracture energy is indeed dissipated computationally.

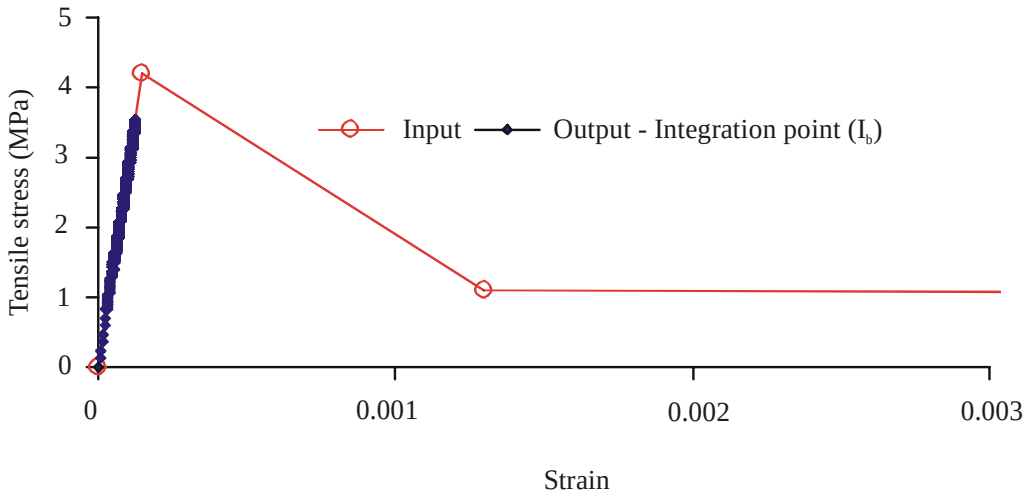

Figure 5-15: Status of tensile stresses in the integration points adjacent to the cracked element.

CHAPTER 6

NON-LINEAR FINITE ELEMENT ANALYSIS FOR SFRC GROUND SLABS

6.1 Introduction

The analysis of SFRC ground slabs represents a complex problem of modelling, due to the non-linearity of the structural response of SFRC, the support and the interaction between the slab and support. For the modelling of SFRC ground slabs, it is not only essential to develop a material model for the slab but it is also critical to develop an appropriate model to represent the behaviour of the underlying support.

In this chapter, analyses are carried out for the SFRC ground slab with particulars given in chapter 3. A finite element model, capable of simulating the non-linear behaviour of the SFRC slab is proposed. An approximate model describing the behaviour of the support layers is developed using results from a plate-bearing test. The same support model is adopted for the analysis of the combined structure of the slab and the support. The material model developed and tested in chapter 5, for the SFRC containing 15 kg/m^3 of steel fibres, is adopted for the analysis of the SFRC slabs.

The developed modelling approach, including the modelling procedure for SFRC and the developed finite element model for ground slabs, is further evaluated by using experimental results for SFRC ground slabs tested by Falkner and Teutsch (1993).

6.2 Modelling the plate-bearing test

The aim of this analysis is to develop an approximate model that describes the overall behaviour of the support layers below the SFRC slab. The support layers are reduced to a single representative slab having the dimensions of the foamed concrete slab. The foamed concrete slab is assumed to rest on a rigid bed. The deformations within the 1000 mm deep, high strength, concrete floor are expected to be insignificant compared to the deformations within the SFRC and foamed concrete slabs. A trial-and-error procedure is followed to estimate a material model for the foamed concrete. The material model of the foamed concrete is changed until calculated and experimental load-displacement (P-Δ) responses are matched. The developed model for the support layers is rather approximate and describes the overall behaviour regardless of the interaction between these support layers (foamed concrete, concrete floor and the soil beneath the concrete floor).

6.2.1 Idealisation of the plate-bearing test

Due to symmetry, only a quarter of the foamed concrete slab is modelled. An equivalent square loading plate, measuring 110 x 110 x 40 mm, is assumed instead of the circular plate used in the experiment. This is to simplify the geometry and thus reduce the calculation required for the finite element analysis. Element type 7 of MSC.Marc is used for the slab and the loading plate. It is a three-dimensional, first order eight-node element. The stiffness of the element is formed using eight-point Gaussian integration. A node in this element has three degrees of freedom; those are displacements in X, Y and Z directions (Δ_X, Δ_Y and Δ_Z). Referring to Figures 6-1, a quarter of the foamed concrete slab is approximated by a finite element mesh consisting of 450 elements while a single element is used for the steel plate. Two layers of 75 mm each were specified for the foamed concrete slab. The displacement of all the nodes at the bottom of the slab are constrained in the Z-direction. The displacements for the nodes at the symmetry planes X = 0 and Y = 0 were constrained in the X-direction and the Y-direction respectively.

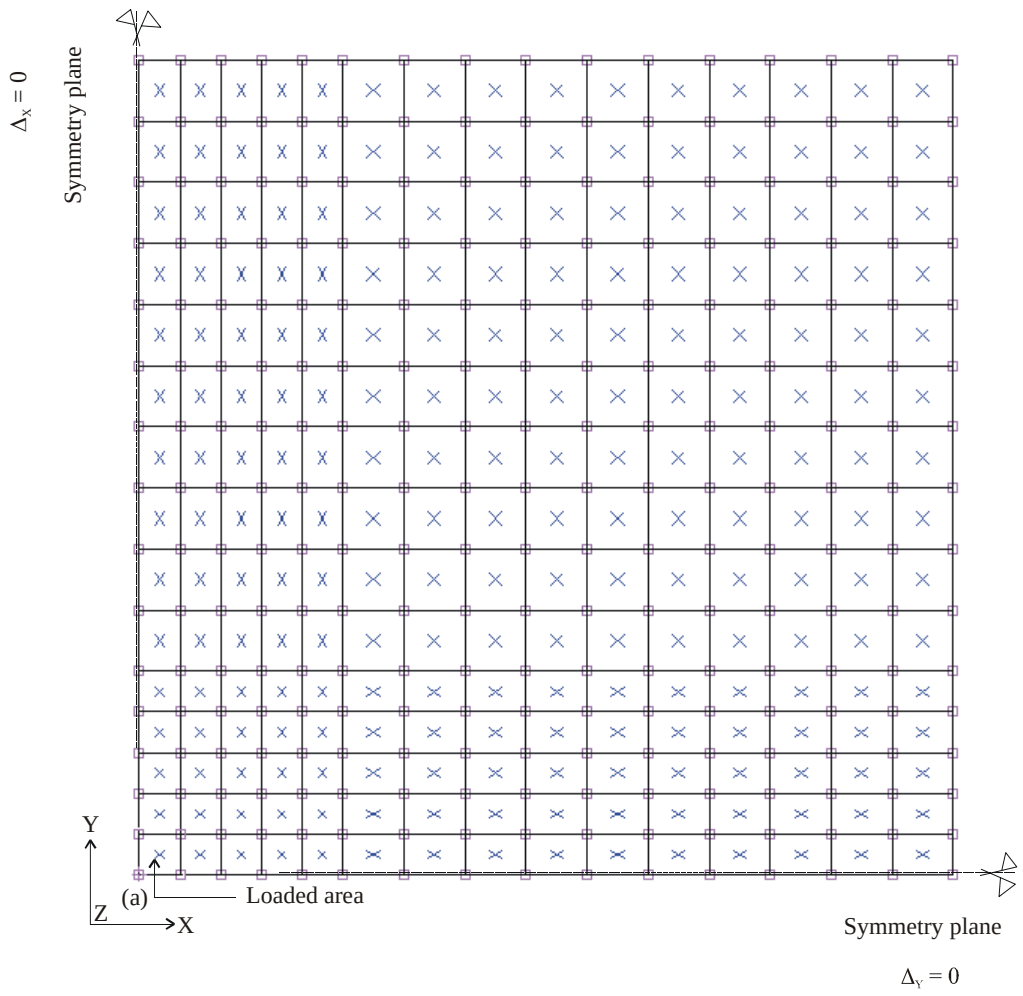

Figure 6-1: The mesh and the boundary conditions for the foamed concrete slab.

The displacement is applied at the centre of the loading plate. The displacement-controlled loading is simulated by increasing the displacement from zero to -10 mm using the time curve concept. The time is divided into five load cases applied consecutively. It should be noted that the reaction of the loading point is equal to a quarter of the applied load as only a quarter of the slab and the steel plate are analysed.

6.2.2 Material model for the support layers

Foamed concrete is basically a hardened cement / binder paste containing high volume of voids. Various percentages of polypropylene fibres are added to improve its shrinkage properties. Under compressive load, the foamed concrete implodes as hardened cement / binder structure collapses to fill the voids within its structure. Compared to normal concrete, the vertical strains are expected to be much larger while lateral strain is much smaller.

A trail-and-error procedure is followed to generate the material model for the foamed concrete slab. A linear elastic compressive σ-ε response is assumed, as in Figure 6-2a. The value of the Young's modulus is changed until the first parts of the calculated and experimental P-Δ responses are matched. A value of 130 MPa and 0.05 was adopted for the Young's modulus and Poisson's ratio respectively. The adopted Young's modulus falls within the range of values suggested by the American Concrete Institute Committee 523 (2000). A relatively low value is arbitrarily assumed for Poisson's ratio, as vertical strains are much larger than lateral strains. Several runs on the model revealed that the value of Poisson's ratio has a little effect.

In the next step a post-yielding part is added to the σ-ε response. The post-yielding part was adjusted following the sequence in Figure 6-2 (b), (c), (d) and (e) until the entire calculated and experimental P-Δ responses are matched as shown in Figure 6-3. The adopted compressive σ-ε response is shown in Figure 6-4. The implosive collapse nature of the foamed concrete suggests that the influence of the lateral pressure is insignificant and therefore, a cylindrical failure surface parallel to hydrostatic axis seems to be appropriate. Accordingly, the Von Mises failure criterion is assumed to govern the multi-axial response of the foamed concrete.

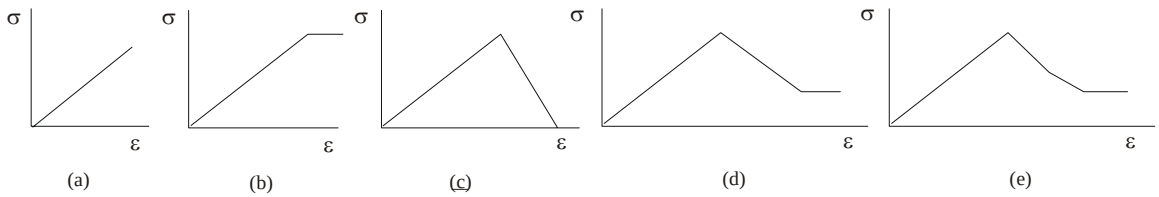

Figure 6-2: Steps followed to generate the stress-strain response for the foamed concrete support.

For the steel plate, a linear elastic response is assumed throughout the analysis. Typical steel characteristics were considered. The values for the Young's modulus and the Poisson's ratio were assumed as 200 GPa and 0.3 respectively. The calculated *P-Δ* response of Figure 6-3 was generated by plotting displacement and four times the reactions of the node (N_2) for the consecutive increments (refer to Figure 6-1).

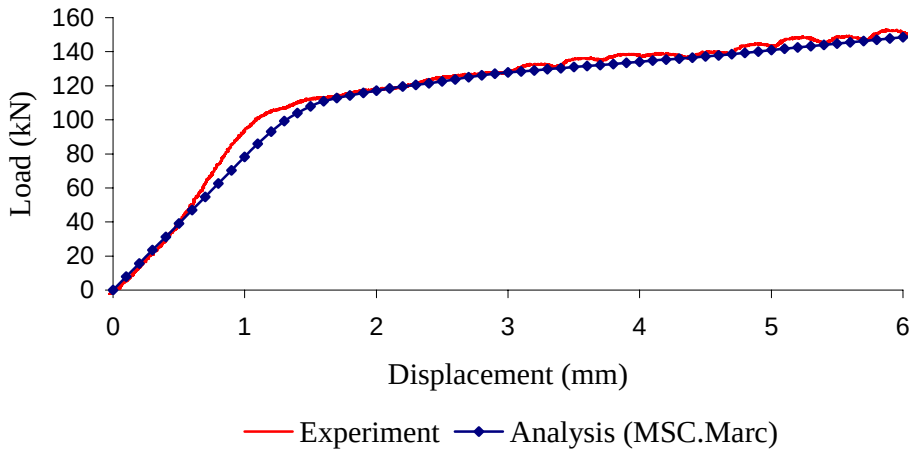

Figure 6-3: Computed and measured load-displacement responses for plate-bearing test.

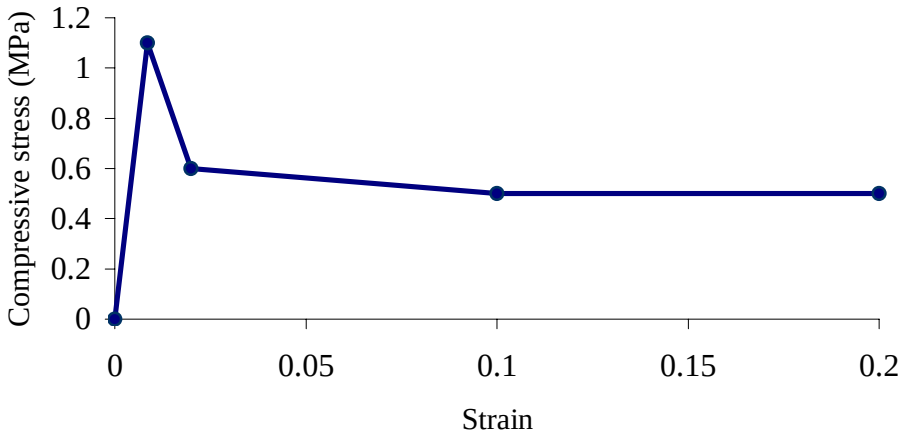

Figure 6-4: The stress-strain response for the foamed concrete support.

Figure 6-4 suggests that the material behaves linear elastic until the peak compressive stress. Thereafter, the stress capacity drops to approximately 55 percent of the peak stress and this stress is sustained to a relatively large strain before complete collapse. The drop in the stress capacity seems relate to the successive collapse of hardened paste filling the voids of foamed concrete. The micro behaviour of foamed concrete is beyond the scope of this study and therefore only the macro

behaviour is considered. Although the foamed concrete material has shown softening in compression, the foamed concrete slab exhibited hardening *P-Δ* response. This is because of the structural ductility associated with slab structure as stresses are being redistributed to the adjacent material. This can be seen in the deformed shape indicated in Figure 6-5.

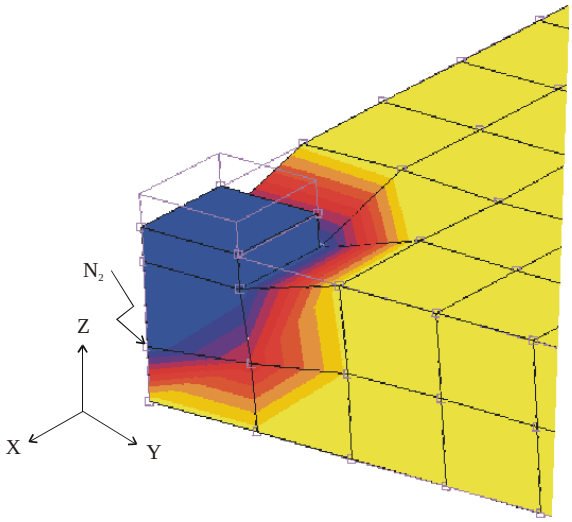

Figure 6-5: The deformed shape of the foamed concrete slab.

Figure 6-6 shows the comparison between the adopted (input) and the output compressive σ-ε responses. The output σ-ε response is extracted at the integration point corresponding to node (N_2) (refer to Figure 6-5). The extracted σ-ε response represents the Von Mises stresses and the total equivalent strains during the consecutive increments. The developed finite element model for the foamed concrete slab, including the material model, the geometry and the boundary conditions, will be used when analysing the SFRC ground slab.

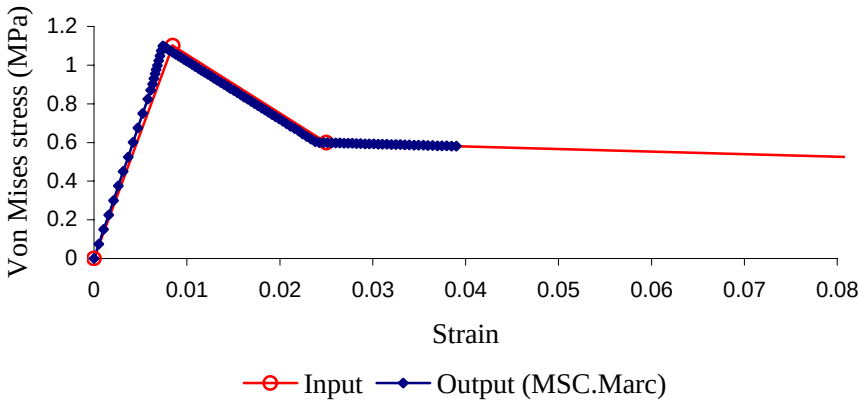

Figure 6-6: Comparison of the input and the output stress-strain responses for the foamed concrete - plate-bearing test.

6.3 Model for SFRC ground slab

The SFRC ground slab presented in chapter 3 will be modelled. The aim is to develop and adjust a finite element model that can be used to model SFRC ground slabs. The model developed in section 6.2 is adopted as a support for the SFRC slab.

6.3.1 Idealisation of the SFRC ground slab

Because of symmetry, only a quarter of the slab is analysed. Element type 75 of MSC.Marc is used. It is a four-node thick shell element with six degrees of freedom per node those are three displacements (Δ_X, Δ_Y and Δ_Z) and three rotations (θ_X, θ_Y and θ_Z). The stiffness of this element is formed using four-point Gaussian integration. It has bending, membrane and transverse shear capabilities which suites the ground slabs applications. The thickness is divided into layers and the stress and stiffness are calculated at representative points through the thickness. The layer number convention is such that layer one lies on the side of the positive normal to the shell, and the last layer is on the side of the negative normal. In many finite element programmes the Mindlin shell theory is implemented resulting in transverse shear distribution being constant through the thickness of the element. In the formulation of element 75 of MSC.Marc, an extension has been made such that a parabolic distribution of transverse shear is used. It is worth noting that this distribution is approximate because it is based on the assumption that the stress in perpendicular directions is independent of each other. The transverse shear strains are calculated at the middle of the edges and interpolated to the integration points of the element.

Figures 6-7 shows the finite element mesh of the SFRC slab. A quarter of the slab is approximated by finite element mesh consisting of 102 shell elements. The thickness of the slab is divided into eleven layers (density of integration points through the thickness equals eleven). A single shell element of type 75 is used for the square loading plate. The displacement of the nodes of the SFRC slab and the loading plate at the symmetry planes X = 0 and Y = 0 were constrained in the X-direction and the Y-direction respectively. The rotation of the nodes of the SFRC slab and the loading plate at the symmetry planes X = 0 and Y = 0 were constrained in the Y-direction and in the X-direction respectively. The rotation of the nodes at the symmetry planes of the SFRC slab and the loading plate were also constrained in the Z-direction. The boundary conditions for the foamed concrete slab remained unchanged. The size of the element used to model the SFRC slab is chosen to be 150 x 150 mm. The selection is made based on the size of the element used when developing the material model for the SFRC. This is necessary because the developed tensile σ-ε response relates to a crack smearing width of 150 mm. The same tensile σ-ε response is applied to the elements having a width of 75 mm. This is because only quarter of the slab is modelled and

therefore half of the fracture energy will be dissipated while cracking occurs in one strip of elements on the centre line through the middle of two opposite edges. The same is assumed for the other strip of elements perpendicular to the first one. In other words only half of the crack is modelled when selecting quarter of the slab model. The two trapezium elements and the 50 x 50 mm element (as indicated in Figure 6-7) were necessary in order to adapt the mesh to the size of the loading plate. The post-cracking part of the tensile σ-ε response therefore needs to be modified for these three elements. Larger element sizes were used at the edges and corner of the slab. The effect of this larger element size is expected to be insignificant on the *P*-Δ response for a slab loaded at its centre.

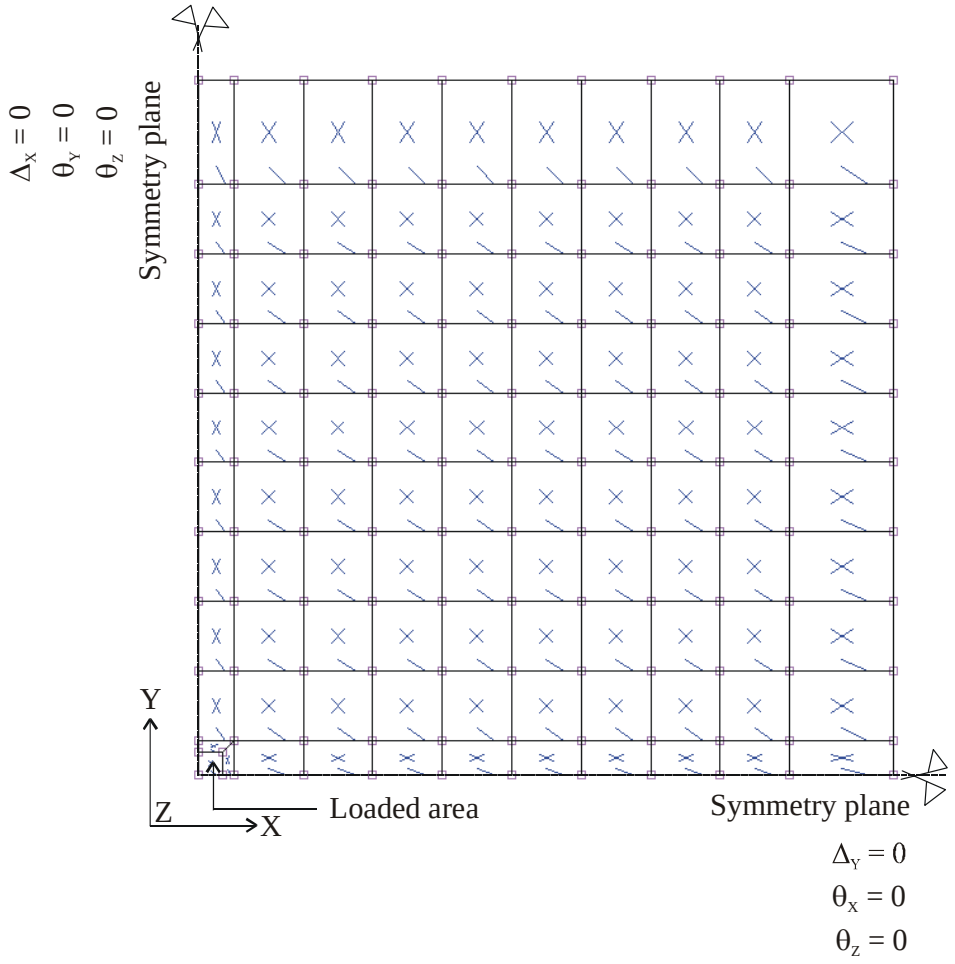

Figure 6-7: The mesh and the boundary conditions for the SFRC slab.

Figure 6-8 shows the loading plate. The nodes of the loading plate are tied to the relevant element (50 x 50 mm) in the SFRC slab. Through this tying, all the displacements and rotations of the SFRC for the particular slab element are set to be dependent on the corresponding nodes of the loading plate.

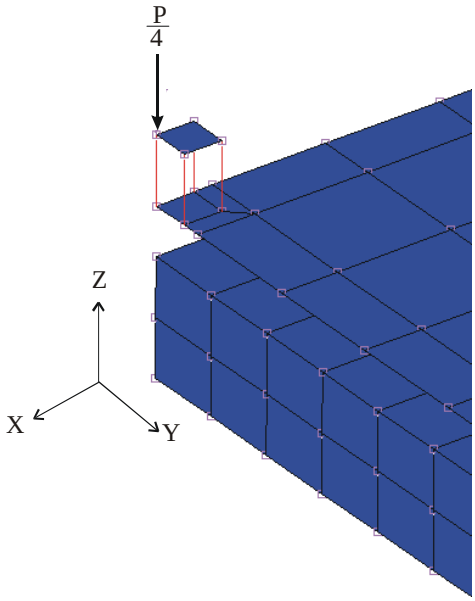

Figure 6-8: The loading plate.

The displacement controlled loading is simulated by increasing the displacement from zero to –10. Smaller increment sizes were applied compared to that used for the analysis of the foamed concrete slab. This is necessary in order to capture the behaviour at the points on the σ-ε response where the slope of the curve changes.

6.3.2 The SFRC slab-support interaction

The contact between the SFRC slab and the support may constitute a domineering feature, especially when plastic deformations are present. The contact between the SFRC slab and the foamed concrete slab was represented by two deformable friction contact bodies with touching contact. A deformable contact body is a set of elements that acts as a body in contact analysis. The deformable contact body can contact other bodies and be contacted by other deformable bodies. During the incremental procedure, each potential contact node is first checked to see whether it is near a contact segment. The contact segments are faces of three-dimensional elements. Touching contact means that two deformable bodies can either be in contact or can be separated. If a node is found to be in contact, the node is constrained in the direction normal and tangential to the contact body. Separation occurs when the tensile contact normal stress on a node in contact becomes larger than the separation threshold stress. The contact is useful to connect independently meshed parts of a structure or to connect two parts of a structure where different types of elements are used (i.e. to connect shell elements and brick elements). For the analysis conducted here, two contact bodies are specified separately for the SFRC slab and the foamed concrete slab. Initially, the SFRC slab is in contact with the foamed concrete slab. A node in the SFRC slab will separate when the tensile contact normal stress exceeds 0.01 MPa. This means that, at a specific node, the SFRC slab loses

contact with the foamed concrete slab when the tensile stress reaches 0.01 MPa and eventually the node does not contribute to the total stiffness of the combined structure of the SFRC slab and the foamed concrete slab. At nodes where the SFRC slab is in contact state with the support the contact has the compressive σ-ε response described in Figure 6-4. The specified value for separation stress (0.01MPa) was decided upon by performing several runs in the model. A friction factor of 0.1 was assumed between the two contact surfaces. A sensitivity study is conducted to evaluate the effect of the separation stress and the friction factor on the P-Δ response of the SFRC slab.

6.3.3 Material model for the SFRC slab

The uniaxial σ-ε response for SFRC in Figure 6-9 is used. In the finite element analysis of the slab, the maximum principal tensile stress will be limited to the values of this tensile σ-ε response. A cracking subroutine is used to allow for the input of the bilinear softening response in MSC.Marc (refer to Appendix C). In the analysis, concrete is assumed to be a linear elastic isotropic material in the pre-cracking stage. A combined criterion is used to simulate the biaxial tensile and compressive behaviour of the SFRC. The crack initiation is governed by the maximum principal tensile stress criterion whereas yielding and plastic behaviour in compression is governed by a Drucker-Prager criterion. A constant shear retention factor of 0.5 is specified to account for the contribution of the shear stresses in the post-cracking stage.

The adopted material model used here is based on a uniaxial response. This material model was found to sufficiently model the behaviour of the SFRC beam as loading of the beam mainly generates uniaxial bending. However, the loading of the SFRC slab is expected to generate a state of biaxial bending. In view of this, it was assumed that a crack in a specific direction does not influence the tensile σ-ε response of the material parallel to the crack. Kupfer (1982) suggested that, under biaxial tension, the strength is almost the same as that of uniaxial tensile strength. Based on this finding, the assumption made here is considered to be adequate.

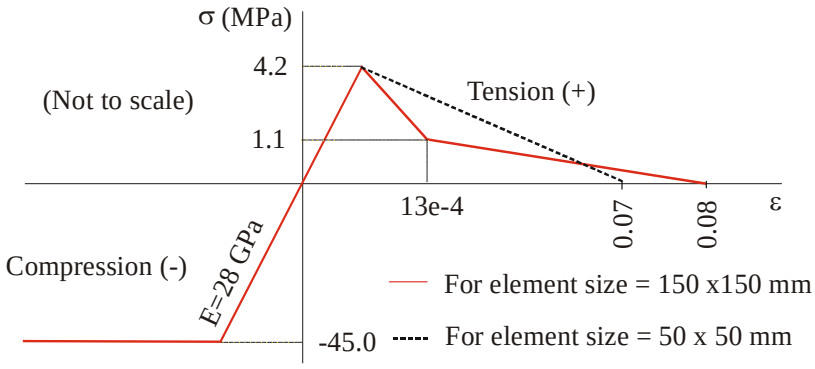

Figure 6-9: The stress-strain response for SFRC containing 15 kg/m^3.

The tensile σ-ε response is adjusted for finite elements smaller than 150 x 150 mm. The adjustment is made for the post-cracking part of the curve based on fracture energy. The dotted line in Figure 6-9 represents the softening response used for the 50 x 50 mm and the trapezium elements. This is not correct for the trapezium elements as their widths ranges between 50 and 150 mm. However, a linear softening response calculated based on the average width (100 mm) of these elements was found to cause insignificant change in the calculated *P-Δ* response. A linear softening response is used for these elements because MSC.Marc only allows for the input of a single cracking subroutine, which was reserved for elements measuring 150 x 150 mm and 75 x 150 mm. The slope for the dotted line of Figure 6-9 is determined by keeping the fracture energy unchanged. The fracture energy can be calculated as the product of the area ($A_{150x150}$) under the softening part of the tensile σ-ε response and the crack smearing width as indicated in Equation 6-1:

$$G_f = 150.A_{150x150} \qquad (6\text{-}1)$$

If the crack smearing width is changed to 100 mm, the area ($A_{100x100}$) under the softening part of the tensile σ-ε response can be calculated as indicated in Equation 6-2:

$$A_{100\,x100} = \frac{G_f}{100}. \qquad (6\text{-}2)$$

The $A_{100x100}$ can be used to determine the ultimate strain and therefore the slope of the linear softening part for the tensile σ-ε response of an element with a width of 100 mm. The same procedure can be followed to calculate the slope of the linear softening part for an element with a width of 50 mm

6.3.4 Results of the finite element analysis of the SFRC ground slab

Figure 6-10 shows the correlation between the calculated and the experimental *P-Δ* responses. The calculated *P-Δ* response is generated by plotting the vertical displacement and four times the reactions at the loading node resulted from consecutive increments (refer to Figure 6-8). The calculated and the experimental *P-Δ* responses reasonably match up to a vertical displacement of approximately 3 mm. The calculated *P-Δ* response deviates significantly from the experimental response beyond this deflection. The load drops after increment 256. The load drop coincides to the extension of the bottom crack from the centre of the slab to the centre of the edges. The calculated *P-Δ* response beyond increment 256 is unrealistic and should be discarded.

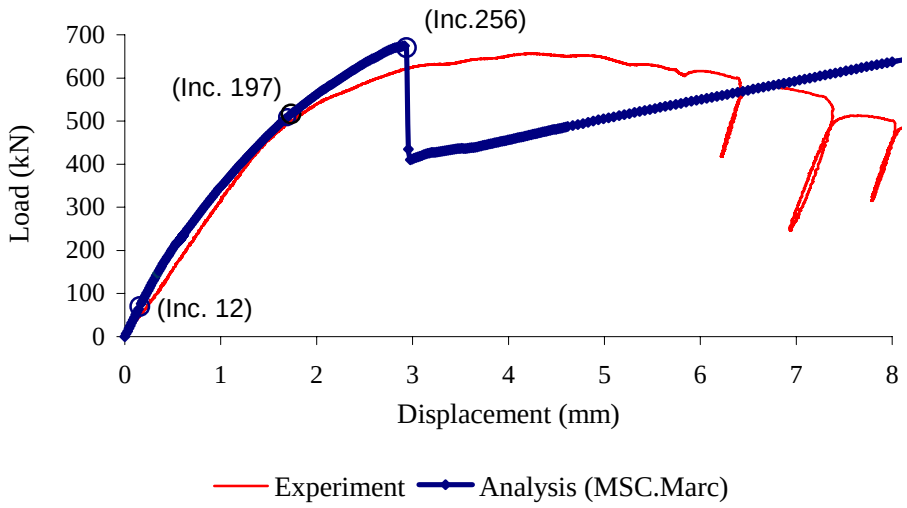

Figure 6-10: Computed and measured load-displacement responses for the SFRC ground slab.

Figure 6-11 shows the deformed shape of the SFRC slab. At increment 256, the centre of the edges and the corner of the SFRC slab moved up by approximately 3.5 mm and 6 mm respectively while the centre moved down by approximately 3 mm. Beyond increment 256 the vertical displacement at the corner increased significantly while the cracks extend from the centre of the slab bottom to the bottom of centres of the edges.

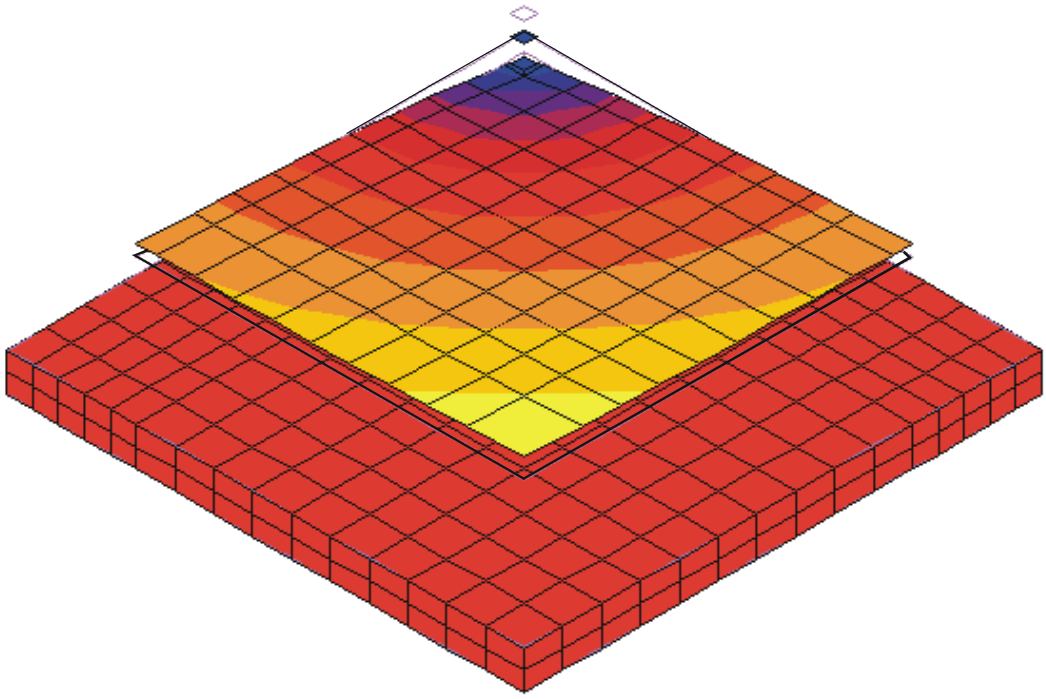

Figure 6-11: Deformed shape of the SFRC slab.

Figure 6-12 shows the progress of cracking in the top surface (layer 1) and bottom surface (layer 11) of the SFRC slab. The initial crack occurred at increment 12 in the bottom of the slab and it is limited to the element below the loading plate and the trapezium elements. The cracking result obtained at increment 12 is not accurate as a slightly different result would be obtained if a bilinear softening response is used for the tensile σ-ε response of these elements (refer to section 6.3.3). The first crack on top of the SFRC slab occurred at increment 197. At increment 256, the crack length increases to surround the loading area, but not to form a complete punching shear mechanism while the bottom cracks extended to the centre of the slab edges. In the ground slab context, these cracks at the bottom and the top of the slab are named as circumferential and radial cracks respectively (Chen, 1982).

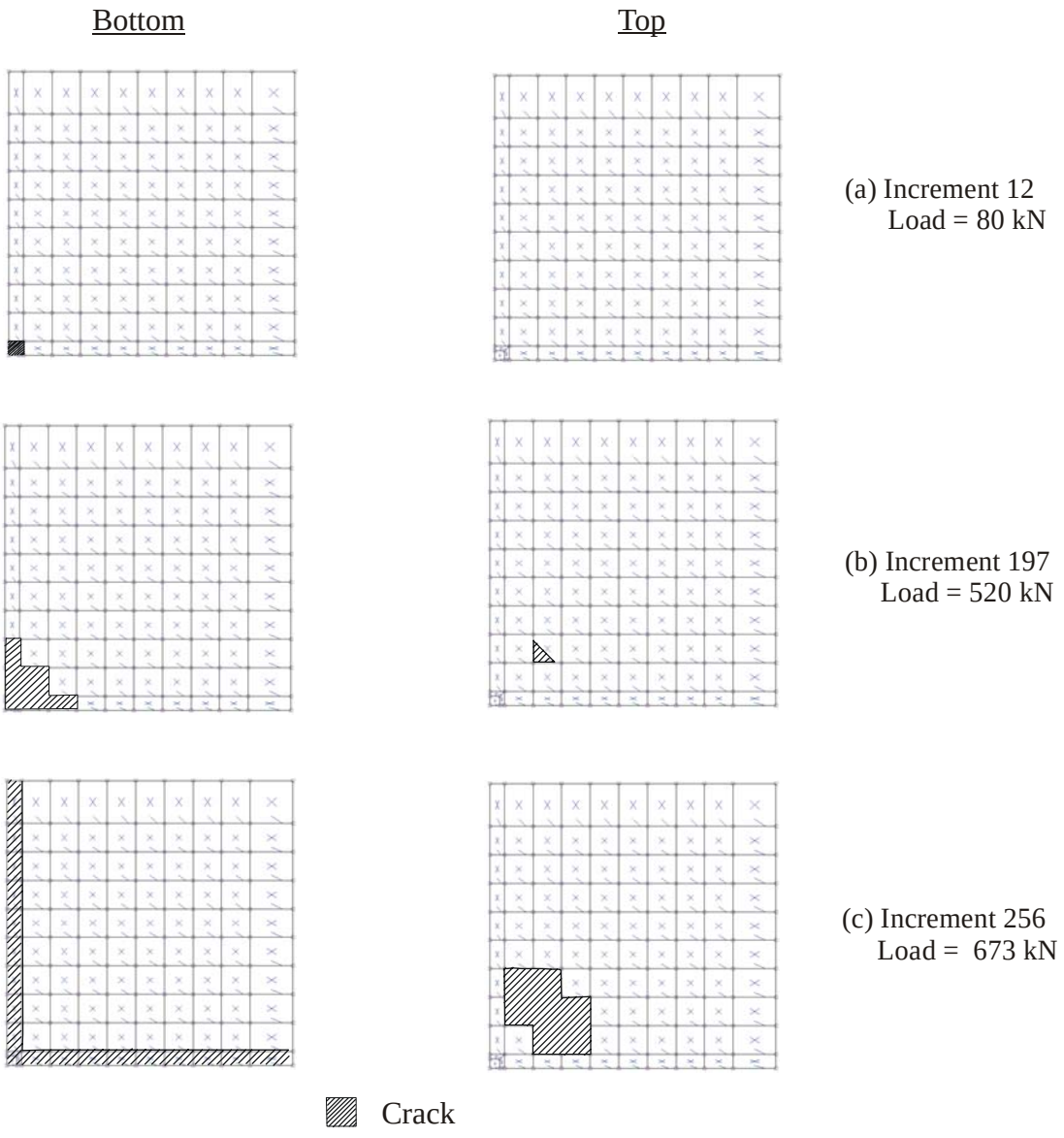

Figure 6-12: The progress of cracking in the SFRC slab.

Figure 6-13 and 6-14 show the comparison between the adopted (input) and the output tensile σ-ε responses of the SFRC slab. The output σ-ε responses were extracted at the integration point of two cracked elements at the bottom and top of the slab. The extracted σ-ε responses represent the maximum principal stresses and strains during the consecutive increments. The input and the output σ-ε responses show good correlation up to a limit. In Figure 6-13, the input and the output σ-ε responses matched until the end of the first softening part of the curve. Thereafter, the output curve starts to deviate significantly from the input. This may attribute to the numerical formulations of the fixed-crack model utilised by MSC.Marc to simulate cracking of low-tension materials. The rotating crack approach is not implemented in the used programme and therefore it is not possible to fully verify this difference. The tensile strain of the finite elements in the top of the SFRC slab was small compared to the strain of the bottom elements (refer to Figure 6-14). The analysis is seen to produce realistic results where the input and the output σ-ε responses match.

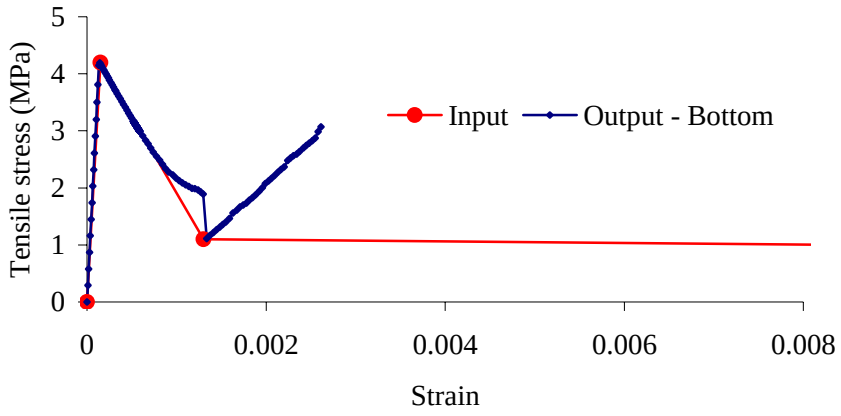

Figure 6-13: The input and the output tensile stress-strain response for the SFRC slab - bottom.

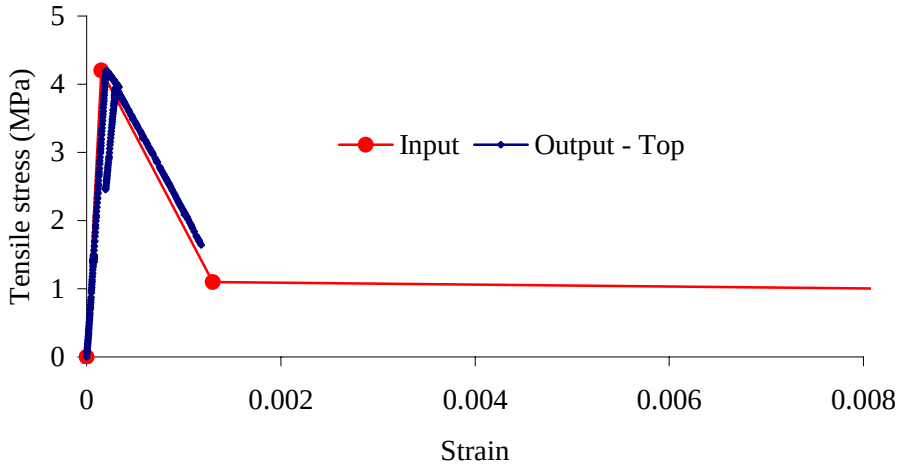

Figure 6-14: The input and the output tensile stress-strain response for the SFRC slab - top.

Figure 6-15 shows the comparison between the adopted (input) and the output compressive σ-ε responses for the foamed concrete slab. The output σ-ε response represents the total strains and the Von Mises stresses extracted at the integration point of a critical element. The input and the output compressive stress-strain responses show good correlation up to the end of the analysis.

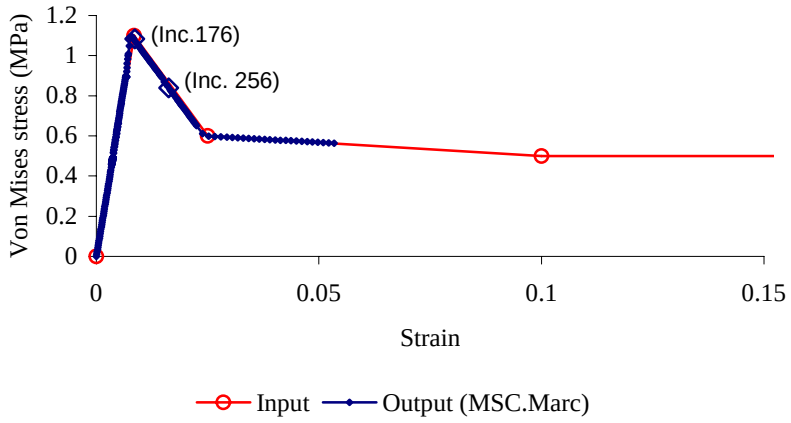

Figure 6-15: The input and output stress-strain responses for the foamed concrete - slab test.

6.3.5 Comments on developed model

The analysis conducted here for the SFRC slab is to appraise the developed constitutive model and finite element model. Care should be taken when selecting the boundary conditions, support characteristics and the load position as well as the load configurations when using the results from this analysis for SFRC pavements. It is necessary to consider the differences between the analysed SFRC slab (model slab) and a pavement slab. For example, lack of edge restraint in the modelled slab allows the slab to lift up at the corner and the edges.

6.3.5.1 Load-carrying capacity of SFRC ground slabs

The developed finite element models for the SFRC slab and for the support (foamed concrete) were used to simulate the experimental behaviour of the supported SFRC slab up to a limit. The results have provided an improved estimation for the load-carrying capacity of the SFRC slab compared to existing theories used for designing SFRC ground slabs. For example, the maximum load calculated for this slab using Meyerhof formulae is approximately 211 kN which is almost three times less than the actual load (650 kN) (refer to Appendix A).

A valuable advantage of the developed non-linear finite element model is that it provides the magnitude of displacement, the extent of the crack and the tensile stress level for each load point on

the P-Δ response. The results obtained from the finite element model can be utilised to design SFRC ground slabs by using one of the following options:

(a) Assume the load-carrying capacity of the SFRC slab is the load at the point of crack initiation keeping in mind that a large factor of safety is provided. For example, the load at initiation of the crack (80 kN) for the analysed SFRC slab means a safety factor of approximately 8.1 is provided. The use of this option is seen to result in an uneconomical design. The crack is found to be localised and does not constitute failure (see Figure 6-12 a).

(b) Assume the load-carrying capacity corresponds to the load causing the first crack in the top surface of the slab. This results in a reduced margin of safety. For example, the first crack on the top surface of the SFRC slab (520 kN) is obtained at increment 197. This means a safety factor of 1.25 is provided. The load-carrying capacity can also be selected in the range of loads between the initiation of the crack in the bottom of the SFRC slab and manifestation of cracks in the top of the slab.

(c) The limit-state philosophy can be implemented by using the peak load achieved in the valid part of the calculated P-Δ response corresponds to the range of increments at which the input and the output σ-ε responses match as the ultimate load-carrying capacity (for example, the load obtained at increment 256). Accordingly, either an un-cracked or a cracked slab will be designed based on the magnitude of the applied safety factor. However, concrete pavement engineers tend to not accept a cracked slab especially if the crack manifests in the surface although the slab can still withstand the load. It is worth noting that the load calculated at increment 256 is approximately 6.7 percent higher than the load obtained at the same displacement from the measured P-Δ response.

(d) The load-carrying capacity and the level of cracking might not be the only limiting criteria. The deflection should also be limited to an acceptable value for some field applications. In the P-Δ response, the load-carrying capacity of the SFRC slab can be chosen based on the load at a prescribed deflection. In the current design practice, deflection criterion does not exist to limit the deflection of a slab.

(e) The load-carrying capacity of a SFRC slab can be based on the fatigue characteristics of the SFRC. This is especially important for SFRC ground slabs subject to repetitive loads. For example, the chosen fatigue model can be used to estimate the tensile stress level (tensile stress divided by the cracking strength), which provides the desired number of load repetitions. The increment

number on the output σ-ε response that relates to the required stress level can be determined. The load at this increment can be read off the calculated P-Δ response.

The developed finite element model can be used in thickness design of SFRC ground slabs. For a given σ-ε response, the finite element model can be used several times to calculate the P-Δ responses for SFRC slabs with different thicknesses. Based on the calculated P-Δ responses and the method used to estimate the load carrying capacity of the ground slab (methods from (a) to (e)), the thickness of the slab can thus be chosen.

6.3.5.2 Cracking of the SFRC slab

The lift of the corners and the centres of the edges shown in Figure 6-11 and the evolution of cracking during the loading process shown in Figure 6-12 indicate that stress redistribution took place after the initial crack occurred in the SFRC slab. The post-cracking strength of the SFRC played a significant role in redistributing these stresses and thus increasing the load-carrying capacity of the SFRC slab. In fact, full advantage of the tensile characteristics of SFRC can only be utilized in statically indeterminate structures where plastic hinges and redistribution can occur.

The failure mechanism was not established while conducting the experiment for the analysed SFRC ground slab, as the purpose of the experiment was only to compare the load-carrying capacity of SFRC to that of plain concrete. However, the results of the finite element analysis conducted here, indicate a failure mechanism similar to the mechanism obtained from an experiment on SFRC ground slabs conducted by Falkner and Teutsch (1993) (refer to Figure 6-16).

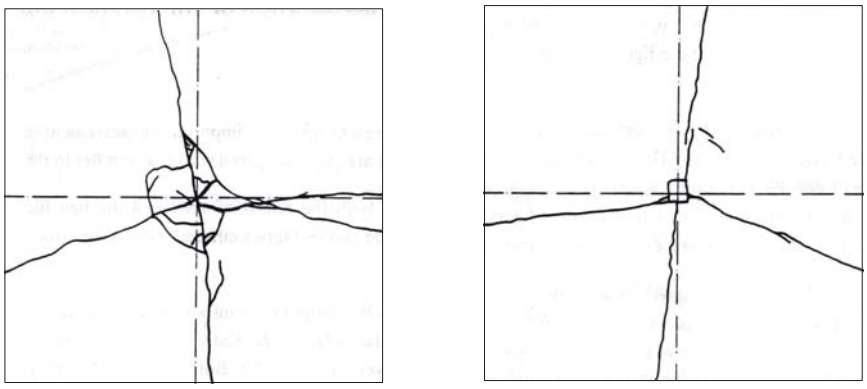

(a) Bottom (b) Top

Figure 6-16: Crack pattern for the SFRC ground slab at failure (Falkner and Teutsch, 1993).

6.3.5.3 Response of the support

Referring to Figure 6-15, the foamed concrete reached the yield point at increment 176. Referring to Figure 6-10, the calculated load corresponding to this increment is 440 kN which lies in the range of loads between the initiation of a crack on the bottom surface and the top surface of the SFRC slab. This can also be seen as a reasonable estimation for the load-carrying capacity of the SFRC slab and can be added to the options (a), (b), (c), (d) and (e) presented in section 6.3.5.

Additional calculations were performed on the developed finite element model using an elastic support. For the linear elastic material, values of 130 MPa and 0.05 were specified for the Young's modulus and the Poisson's ration ratio respectively (same values used for the actual σ-ε response in Figure 6-15). A relatively high elastic strain is specified to allow the material to deform elastically up to a relatively high strain (refer to Figure 6-17).

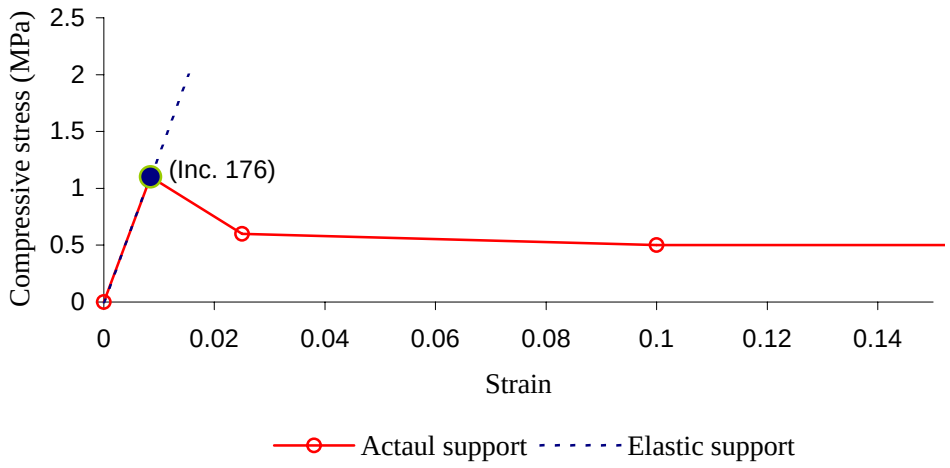

Figure 6-17: Elastic and actual stress-strain response used for foamed concrete.

Figure 6-18 shows the comparison between the measured and the calculated P-Δ responses. The calculated P-Δ responses using actual support and elastic support match up to increment 191. In spite of the difference in the σ-ε responses beyond increment 176, the calculated P-Δ responses match up to increment 191. It can be deduced that the P-Δ behaviour of the SFRC ground slab between increment 176 and 191 is more influenced by the characteristics of the SFRC slab than the characteristics of the foamed concrete. Beyond increment 191 the characteristics of the support starts to dominate the behaviour of the SFRC ground slab. The maximum load calculated using the elastic support is approximately 32 percent higher than the load obtained at the same displacement from the experimental P-Δ response. This percentage is expected to reduce if a softer support and /

or higher strength concrete and steel fibre content is used for the SFRC ground slab. Keeping in mind these factors, an elastic support can successfully be used for the support layers to obtain satisfactory results from the finite element analysis of SFRC ground slabs.

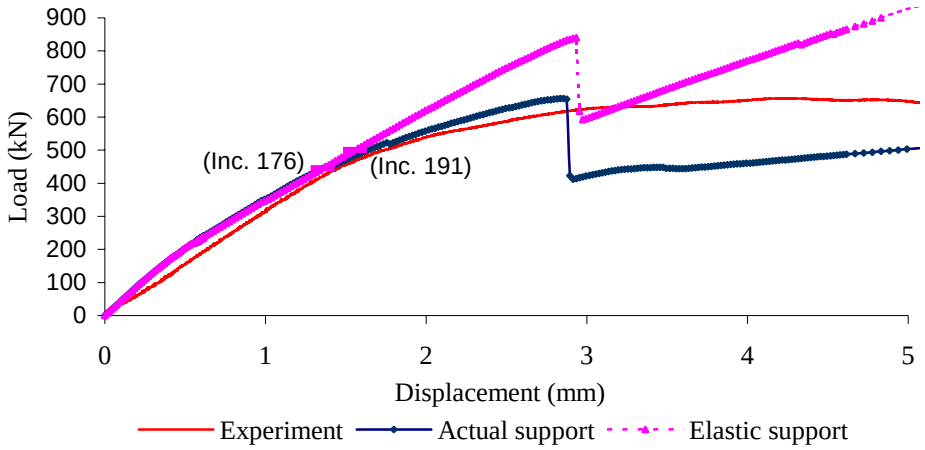

Figure 6-18: Comparison of load-displacement responses for the SFRC ground slab using elastic and actual support models.

Figure 6-19 shows the effect of the friction factor on the *P-Δ* response of the SFRC ground slab. The friction between the slab and the support seems to have insignificant effect on the behaviour of a ground slab loaded at its centre.

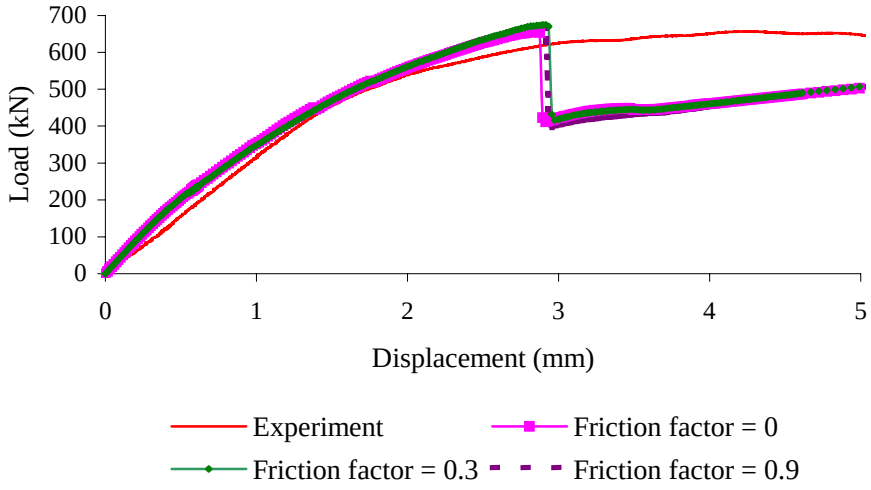

Figure 6-19: Effect of the friction factor on the load-displacement response of SFRC ground slab.

Figure 6-20 shows the effect of the separation stress on the *P-Δ* response of the SFRC ground slab. The separation stress seems to have significant effect on the behaviour of the slab. A value of 0.1 MPa or higher results in the SFRC and the foamed concrete slab to act as one element and therefore increases the load-carrying capacity. A value of 0.01 or less causes the SFRC slab to lift up and therefore provides *P-Δ* response that matches the experimental response.

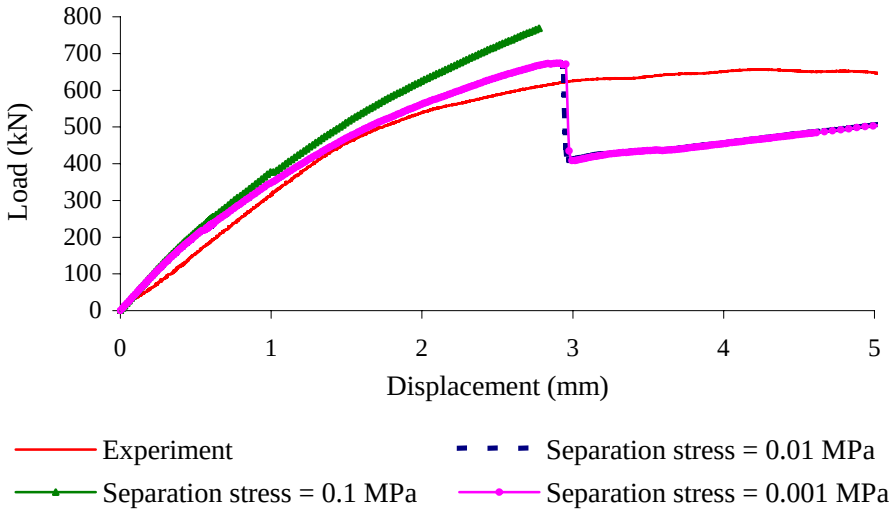

Figure 6-20: Effect of the separation stress on the load-displacement response of SFRC ground slab.

6.4 Implementation of the modelling approach on ground slabs tested by other agencies

The analytical approach used to calculate the tensile σ-ε response for SFRC and the developed finite element model for the SFRC ground slabs were further evaluated. The experimental results of SFRC ground slabs tested by Falkner and Teutsch (1993) are utilised. In their experimental programme, slabs measuring 3000 x 3000 x 150 mm and beams measuring 700 x 150 x150 mm were manufactured and tested. The slabs were either cast on elastic cork or rubber that was 60 mm thick and was placed on a rigid testing floor.

The slabs were centrally loaded via a hydraulic jack on a steel plate measuring 120 x 120 mm. Only experimental results relevant to the SFRC ground slabs P3 and P4 are discussed here. The experimental results of the *P-Δ* responses and the deformation profiles, on the cross-section between the centres of the parallel edges of the slab, are compared to the theoretical results. The properties for these two slabs are shown in Table 6-1.

Table 6-1: Properties of the SFRC ground slabs tested by Falkner and Teutsch (1993).

Property	Slab P3	Slab P4
Steel fibre content (kg/m^3) - hooked-end	20	20
Average compressive strength of SFRC (MPa)	39.9	45.1
Young's modulus of SFRC (GPa)	23.4	26.65
Young's modulus of subbase material (MPa)	1.4 (Cork)	6.0 (Rubber)

The P-δ responses of the beams made from the parent SFRC mix of slab P3 and slab P4 were used to calculate the σ-ε response. The average compressive strengths and the Young's modulus are given in Table 6-1. The method proposed in chapter 4 is used. The setup for the beam tests is shown in Figure 6-21. The calculated σ-ε responses and the comparison between the measured and the calculated P-δ responses for slab P3 and P4 are indicated in Appendix D.

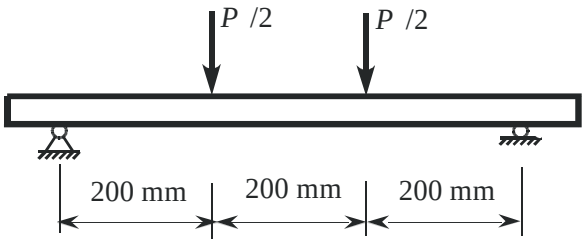

Beam cross-section 150 x 150 mm

Figure 6-21: Test set-up for the beams tested by Falkner and Teutsch (1993).

For the calculated σ-ε responses, the crack is smeared over a width of 200 mm (the width between the applied loads). Accordingly, the size of the finite element is chosen to be 200 x 200 mm. Figure 6-22 shows the finite element mesh and boundary conditions for a quarter of the slabs. An adjustment is made to the σ-ε responses for the 60 x 60 mm, the trapezium and the edge elements in a similar manner as in section 6.3.3. Elastic supports having a Young's modulus of 1.4 and 6.0 MPa were used for slab P3 and P4 respectively. Poisson's ratio is assumed to be 0.35 for the cork and the rubber. The rest of the details of the finite element analysis are kept the same as those explained in section 6.3.

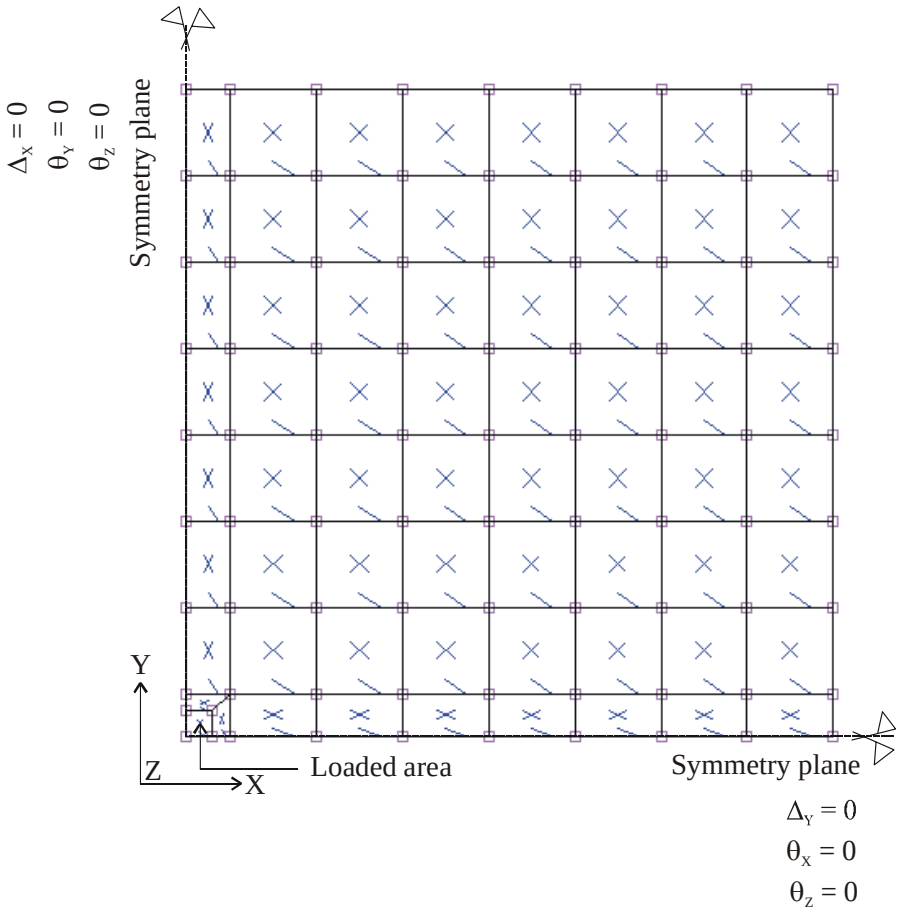

Figure 6-22: The mesh and the boundary conditions for the SFRC slabs tested by Falkner and Teutsch (1993).

Figure 6-23 and Figure 6-24 show that the calculated and the experimental *P-Δ* responses reasonably match up to a vertical displacement of approximately 3.8 and 2.5 mm for slab P3 and P4 respectively.

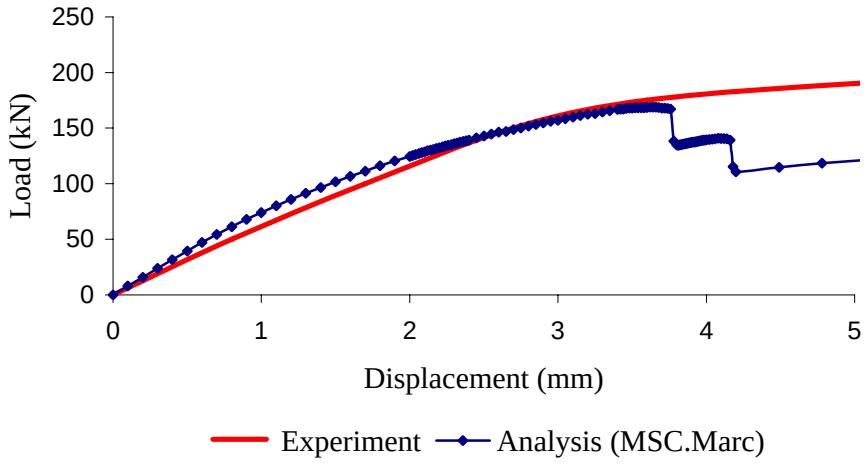

Figure 6-23: Computed and measured load-displacement responses for the SFRC ground slab P3.

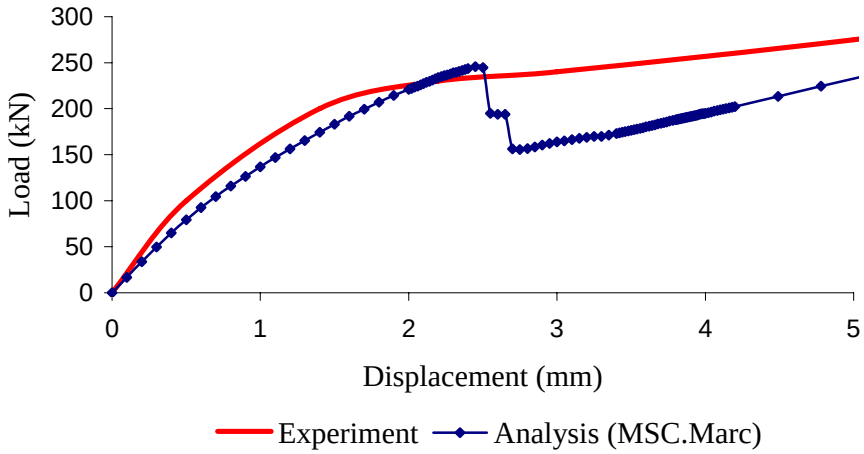

Figure 6-24: Computed and measured load-displacement responses for the SFRC ground slab P4.

In Figure 6-25 and Figure 6-26 the measured and the calculated profiles of the cross-section of the slab between the centres of the parallel edges are compared for slabs P3 and P4 respectively. The developed finite element model can not only be used to simulate the *P-Δ* response at the loading point, but it can also be used to simulate the behaviour of the slabs at a distance from the loading point. The material modelling approach for the SFRC and the developed finite element model can be successfully used to simulate the non-linear behaviour of SFRC ground slabs.

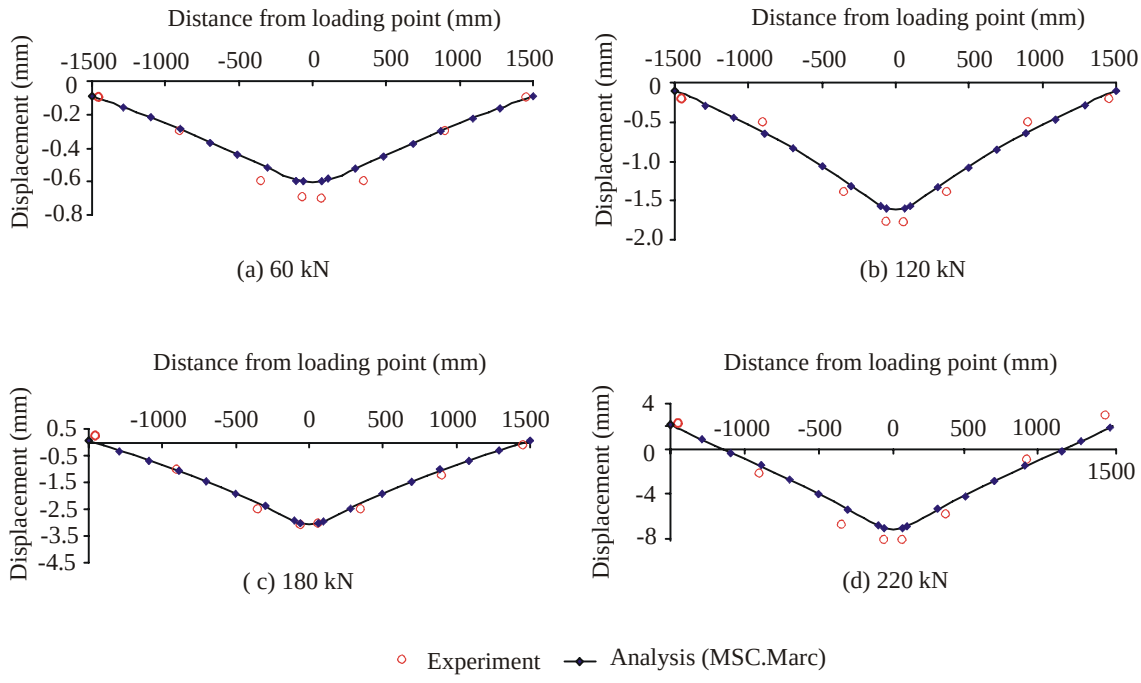

Figure 6-25: Profiles on cross-section between the centres of edges of slab P3.

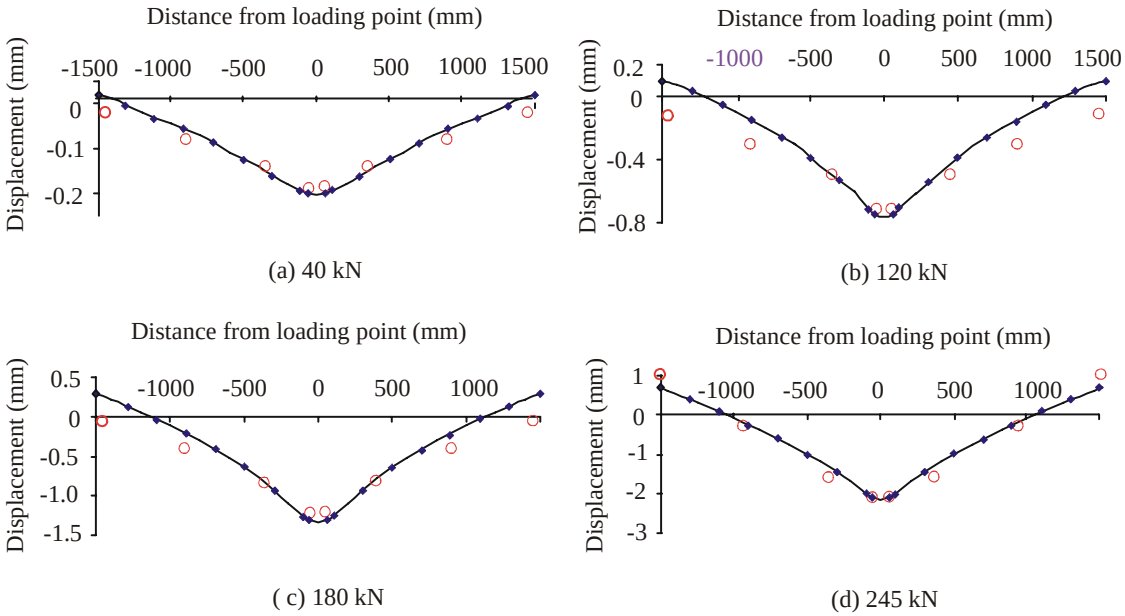

Figure 6-26: Profiles on cross-section between the centres of edges of slab P4.